Advances in Colloid and Interface Science 166 (2011) 8–23

Contents lists available at ScienceDirect

Advances in Colloid and Interface Science

journal homepage: www.elsevier.com/locate/cis

Magnetic fluid hyperthermia: Focus on superparamagnetic iron oxide nanoparticles

Sophie Laurent [a], Silvio Dutz [b,c], Urs O. Häfeli [b], Morteza Mahmoudi [d,e,*]

[a] Department of General, Organic, and Biomedical Chemistry, NMR and Molecular Imaging Laboratory, University of Mons, Avenue Maistriau, 19, B-7000 Mons, Belgium
[b] Faculty of Pharmaceutical Sciences, The University of British Columbia, Vancouver, Canada
[c] Department Nano Biophotonics, Institute of Photonic Technology, Jena, Germany
[d] National Cell Bank, Pasteur Institute of Iran, Tehran, Iran
[e] Nanotechnology Research Center, Faculty of Pharmacy, Tehran University of Medical Sciences, Tehran, Iran

ARTICLE INFO

Available online 30 April 2011

Keywords:
Superparamagnetic iron oxide nanoparticles
Physiochemical properties
Cancer
Hyperthermia
Theragnostics

ABSTRACT

Due to their unique magnetic properties, excellent biocompatibility as well as multi-purpose biomedical potential (e.g., applications in cancer therapy and general drug delivery), superparamagnetic iron oxide nanoparticles (SPIONs) are attracting increasing attention in both pharmaceutical and industrial communities. The precise control of the physiochemical properties of these magnetic systems is crucial for hyperthermia applications, as the induced heat is highly dependent on these properties. In this review, the limitations and recent advances in the development of superparamagnetic iron oxide nanoparticles for hyperthermia are presented.

Contents

1. Introduction

Magnetic nanoparticles (MNP) have found numerous applications in biomedicine, such as magnetic separation, drug delivery, magnetic resonance imaging (MRI), and hyperthermia [1–4]. Due to rapid advances in nanotechnology, novel synthetic routes to nanoparticles (NPs) with the ability to rigorously control the microstructure of the magnetic core (such as size monodispersity and crystallinity) have been described [5–9]. These nanosystems can be made to heat up, which leads to their use as hyperthermia agents, delivering toxic amounts of thermal energy to tumors, or as chemotherapy and radiotherapy enhancement agents, where a moderate degree of tissue warming results in more effective cell destruction [10]. The increasing interest for MNP is due to the discovery of their physical and chemical properties. In particular, it has been shown that the magnetic anisotropy of MNP can be much greater than those of a bulk specimen, while differences in the Curie or Néel temperatures, i.e., the temperatures of spontaneous parallel or antiparallel orientation of spins between MNP and the corresponding microscopic phases, reach hundreds of degrees [11]. In addition, magnetic nanomaterials have been found to possess a number of interesting properties such as giant magnetoresistance or abnormally high magnetocaloric effect.

* Corresponding author.
E-mail address: mahmoudi@biospion.com (M. Mahmoudi).
URL: http://www.biospion.com (M. Mahmoudi).

0001-8686/$ – see front matter © 2011 Elsevier B.V. All rights reserved.
doi:10.1016/j.cis.2011.04.003

Experimental investigations of the application of magnetic materials for hyperthermia date back to 1957 when Gilchrist et al. [12] heated various tissue samples with 20–100 nm size particles of γ-Fe_2O_3 exposed to a 1.2 MHz magnetic field. Since then, there have been numerous publications describing a variety of schemes using different types of magnetic materials, different field strengths and frequencies, and different methods of encapsulation and delivery of the particles [13].

The application of ferrofluids for hyperthermia treatment was investigated in the work of Chan et al. [14] and Jordan et al. [15] in 1993. These studies experimentally prove the high efficiency of a superparamagnetic crystal suspension to absorb the energy of an alternating magnetic field and convert it into heat. Given that tumor cells are more sensitive to a temperature increase than healthy ones [16,17], this property can be used in vivo to increase the temperature of tumor tissue and to destroy the pathological cells by hyperthermia.

Many efforts have been devoted in the last 20 years to improve hyperthermia techniques for clinical applications. Advances in the area of nanotechnology have contributed to the development of magnetic fluid hyperthermia. This technique is a promising technique for cancer treatment because of ease in targeting the cancerous tissue and hence having fewer side effects than chemotherapy and radiotherapy. It is notable that the results of current/ongoing clinical trials show significant reduction in side effects [18].

One of the early magnetic fluid papers for magnetic hyperthermia. They injected 100 mg dextran magnetite into the tail vein of Sprague–Dawley rats, treated with AC magnetic field (12 min, 450 kHz, unknown field and SAR), and saw tumor shrinkage and tissue necrosis. After this, they just published a few patents until 1988 [19]. Flow of embolized carbonyl iron particles under the influence of a magnetic field was evaluated in vitro and in vivo. The magnetic force caused particles to form aggregates, obstructing tubing or vascular beds. In dogs, 0.5 ml of iron particles injected into a renal artery under magnetic control may be helpful in embolic arterial occlusion and localized irradiation, hyperthermia and chemotherapy [20]. Rand et al. [21,22] introduced additional radiofrequency heating up to more than 55 °C on the renal surface of rabbits. In this way, total coagulation necrosis of a renal cancer model could be achieved, possibly more as a result of the hyperthermic treatment than caused by the occlusion. The treated animals survived the procedures and exposure in the magnetic field and to the ferromagnetic compounds without evidence of ill effects.

The first clinical patient trials [23] were started by the research group of Jordan [24–38]. They built a hyperthermia-generating prototype instrument which is able to generate variable magnetic fields in the range of 0–15 kA/m at a frequency of 100 kHz. At the same time, the machine allows for real time patient temperature measurements to ensure that neither the upper limit of the therapeutic temperature threshold is exceeded, thus preventing thermal ablation, nor the lower, ineffective limit is crossed. This prototype is capable of treating tumors placed in any region of the body (e.g., prostate cancer, brain tumors).

Currently, only local hyperthermia is considered for magnetic fluid hyperthermia. For this purpose, MNP in a carrier fluid are placed inside the tumor through direct injection or tumor specific antibody targeting, after which the tumor is exposed to an alternating magnetic field. This field makes the particles generate heat by magnetic relaxation mechanisms. For hyperthermia treatments knowing the temperature profile obtained in the tissues is of utmost importance. The ideal temperature profile is one where the body temperature in healthy tissue is maintained, while the therapeutic temperature of 45 °C inside the tumor is reached immediately and maintained constant. In reality these temperature profiles are not flat, neither in the tumor nor in normal tissue, because of thermal diffusion.

In this review, we will focus on the basic concepts of magnetism and review the physics of the hyperthermia process.

2. Physics of magnetism

When a magnetic material is placed in a magnetic field of strength H, the individual atomic moments in the material contribute to its overall response; the magnetic induction is given by Eq. (1):

$$B = \mu_0(H + M) \tag{1}$$

where μ_0 is the permeability in vacuum and M is the magnetic moment per volume. The magnetic materials may be conveniently classified in terms of their volumetric magnetic susceptibility, χ (with $M = \chi H$). Most materials display magnetism only in the presence of an applied field. They are classified as paramagnets, with χ in the range of 10^{-6}–10^{-1}, or diamagnets with a negative χ. However, some materials exhibit ordered magnetic states and are magnetic without requiring a magnetic field; these are classified as ferromagnets, and ferrimagnets [40]. The coupling interaction between magnetic moments within the material can give rise to large spontaneous magnetizations.

In 1930, Frenkel and Dorfman [41] showed on the basis of energy considerations that particles of a sufficiently small size should be single-domain. In the mid-20th century, the theory of single-domain particles started to be actively developed [42–45] and the related phenomena were studied experimentally [46–53]. These studies identified a substantial increase in the coercive force of a ferromagnet on passing from a multi-domain to the single-domain structure, which is important for the creation of permanent magnets. The calculated critical diameter (at room temperature) of a single-domain spherical particle with axial magnetic anisotropy varies in a broad range. The upper values are 128 nm for Fe_3O_4 and 166 nm for γ-Fe_2O_3 [54] and the lower values are around 80 nm for magnetite [55]. The latter data were confirmed experimentally for particles consisting of solid solutions of maghemite and magnetite [56]. Experimental determination of the critical diameter above which a single-domain particle becomes multi-domain is a complicated task, although it has recently become possible to observe this transition directly through a magnetic force microscope [57,58] or a quantum magnetic interferometer (m-SQUID) [59–61] or indirectly by means of the analysis of the magnetic properties.

The term 'single-domain' does not require a uniform magnetization throughout the whole particle bulk but only implies the absence of domain walls. The specific properties of MNP start to be manifested at sizes much smaller than the 'single-domain limit'.

One more remarkable property of MNP, which allowed their experimental discovery in the mid-20th century, is their superparamagnetism. The model of an ideal superparamagnetic material was proposed in the early 1960s [62], but is still under development [63,64]. The simplest variant of this model considers a system of N non-interacting identical particles with the magnetic moment μ_{ef}. Since the magnetic moment of the particle is assumed to be large, its interaction with the magnetic field H is calculated without taking into account the quantum effects. In the case of isotropic particles, the equilibrium magnetization of the [M] system can be described by the Langevin equation (Eq. (2)):

$$\langle M \rangle = N\mu_{ef}\left[cth\left(\frac{\mu_{ef}H}{k_BT}\right) - \frac{k_BT}{\mu_{ef}H}\right] \tag{2}$$

Eq. (2) has been derived with the assumption that single particles are magnetically isotropic, i.e., all directions of their magnetic moments are energetically equivalent, but this condition is hardly ever fulfilled. If the particles are magnetically anisotropic, the calculation of the equilibrium magnetization becomes more complicated. According to the nature of factors giving rise to the non-equivalence of the directions of magnetic moments, one can distinguish the magnetically crystalline anisotropy,

the shape anisotropy, anisotropy associated with the internal stress and external impact, and the exchange anisotropy [65].

For MNP, the surface magnetic anisotropy plays a special role. Unlike other kinds of magnetic anisotropy, surface anisotropy is proportional to the surface area of the particle rather than to its volume. Surface anisotropy appears due to the violation of the local environment's symmetry and the change in the crystal's field, which acts on magnetic ions located on the surface.

Uniaxial anisotropy is the simplest type of magnetic anisotropy. In general, the equation for the energy of uniaxial magnetic anisotropy is written as the sum of two contributions (Eq. (3)):

$$E(\theta) = (K_V V + K_S S)\, sin^2\theta \tag{3}$$

where K_V is the volume anisotropy constant, V is the particle's volume, K_S is the surface anisotropy constant, S is the particle's surface and θ is the angle between the vector of the particle's magnetic moment m and the anisotropy axis.

When the surface makes no contribution to the anisotropy, the angular dependence of the particle energy has the form given in Eq. (4):

$$E(\theta) = K_V V\, sin^2\theta \tag{4}$$

If no external magnetic field or surface anisotropy is present, the minimum energy of the particle is attained at the orientation of the magnetic moment M along the easy magnetocrystalline anisotropy axis. In this case, two neighboring minima are separated by a barrier with height $K_V V$. In an external magnetic field H applied at the angle ψ to the anisotropy axis, the particle's energy is defined by Eq. (5):

$$E(\theta) = K_V V sin^2\theta - M_s V H cos(\theta - \psi) \tag{5}$$

Generally, in the presence of an external magnetic field, rotation of the particle's magnetic moment to reach the orientation corresponding to a minimum energy, requires overcoming an energy barrier, $\Delta E \sim K_V V$. The relation for the characteristic time of thermal fluctuations of the magnetic moment of a single-domain particle with uniaxial anisotropy provided that $\Delta E/k_B T \geq 1$ was obtained by Néel (Eq. (6)) [44]:

$$\tau = \tau_0 e^{\left(\frac{\Delta E}{k_B T}\right)} \tag{6}$$

Later, Eq. (6) was extended by Brown [45] to the cubic anisotropy case.

The pre-exponential factor τ_0, is an expression of the anisotropy energy and depends on many parameters, including temperature, gyromagnetic ratios, saturation magnetization, anisotropy constants, the height of energy barrier, etc. [66–68]. However, for the sake of simplicity τ_0 is often considered to be a constant in the range of 10^{-9} to 10^{-13} s [54]. Eq. (6) determines the characteristic time needed to establish the thermal equilibrium in a system of non-interacting single-domain magnetic particles. At higher temperatures, $\Delta E/k_B T \ll 1$, the time required for system transition into a state with the minimum energy is short compared to the characteristic time of measurements τ_{meas}, and the system is not expected to show a magnetic hysteresis. In the case of $\Delta E/k_B T \gg 1$, the system transition into an equilibrium state may take a very long time depending appreciably on the particle. If $\tau_{meas} \gg \tau$, the system occurs in the superparamagnetic state and rapidly reaches an equilibrium magnetization on changing the temperature or the external field. With a $\tau_{meas} \ll \tau$, however, after a change of the external magnetic field, the system does not arrive at a new equilibrium state over the time τ_{meas} and its magnetization does not change. The case $\tau = \tau_{meas}$ in Eq. (6) corresponds to the blocking temperature T_b. If $\tau_{meas} = 100$ s (characteristic time for the static magnetic measurements) and $\tau_0 = 10^{-9}$ s, the condition $\tau_{meas} = \tau$ in relation (6) gives $K_V V \sim 25.3\, k_B T$.

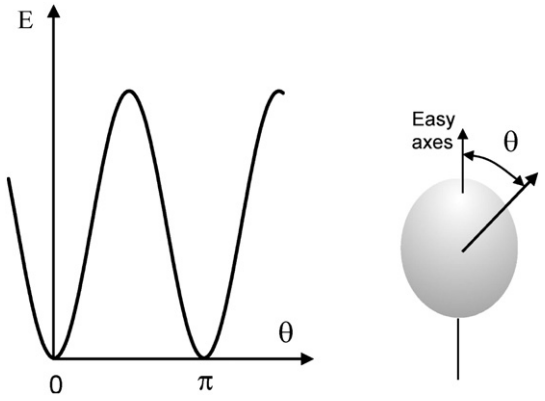

Fig. 1. Evolution of the magnetic energy with the tilt angle between the easy axis. Reproduced from Ref. [1].

As the external magnetic field is enhanced, the blocking temperature decreases by a power law (Eq. (7)):

$$T_b(H) = T_b(0)\left(1 - \frac{H}{H_c}\right)^k \tag{7}$$

where $k = 2$ (for low fields [69]) and $k = 2/3$ (for high fields [70]), and $H_c = 2K/M_s$.

Fig. 1 shows the dependency of magnetic energy of a nanomagnet upon the direction of its magnetization vector. The directions that minimize this magnetic energy are called anisotropy directions or easy axes. The magnetic energy increases with the tilt angle between the magnetization vector and the easy directions. The variation amplitude of this curve is called anisotropy energy [1].

For a dry powder of monodomain particles, the Néel relaxation time is characterized by the time constant of the return to equilibrium of the magnetization after a perturbation. In high anisotropy conditions, the crystal magnetization is locked in the easy axes which favor the direction of less magnetic energy. The Néel relaxation defines then the fluctuations that arise from the jumps of the magnetic moment between different easy directions. Brownian relaxation characterizes the viscous rotation of entire particles [1]. Fig. 2 shows the two components of the magnetic relaxation of a magnetic fluid.

To investigate the magnetic properties of samples containing MNP, the magnetization curve is usually measured up to saturation [71]. In order to determine the temperature dependence of the magnetic

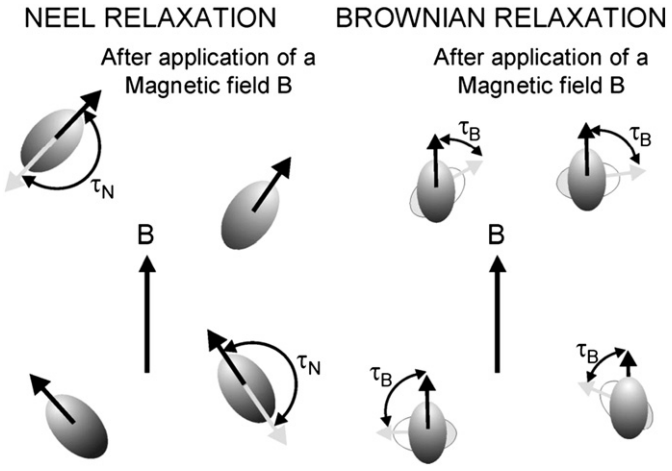

Fig. 2. Illustration of the two components of the magnetic relaxation of a magnetic fluid.

moment M, two types of measurements are carried out; namely, zero-field cooling (ZFC) and field cooling (FC). According to the ZFC procedure, the sample is cooled (usually down to the liquid helium temperature) in the absence of a magnetic field and then a moderate measuring field is applied and the temperature is gradually raised, while the magnetic moment m_{ZFC} values are being recorded. The FC procedure differs from ZFC only by the fact that the sample is cooled in a non-zero magnetic field. For MNP, the M_{FC} (T) and M_{ZFC} (T) curves usually coincide at relatively high temperatures but start to differ below a certain temperature T_{ir} (irreversibility temperature). The M_{ZFC} (T) curve has a maximum at some temperature T_{max}, and the M_{FC} (T) curve, most often, ascends monotonically to very low temperatures. The dependence of magnetization on the applied field at various temperatures is often measured as well [72]. Electron magnetic resonance and Mossbauer spectroscopy data are also used to analyze the magnetic properties.

3. Magnetic heating

The classical approach of hyperthermia consists of submitting the patient to electromagnetic waves of several hundred MHz frequencies. The thermoablation of a tumor can be achieved by an electromagnetic wave emitted by a RF electrode implanted in the pathological area. A less invasive method consists of irradiating the pathological area with an array of external resonant microwave dipolar emitters [73–75]. Preclinical and clinical data show that hyperthermia is feasible and effective in combination with radiation therapy. A study of 112 patients with glioblastoma multiformae showed that that median survival times increased significantly from 76 to 85 weeks, while 2-year survival jumped from 15% to 31% when γ-therapy was combined with hyperthermia as compared to γ-therapy alone [76]. One important contribution of the hyperthermia treatment is the increase of perfusion in the tumor tissue which also increases the local oxygen concentration and thus results in optimal conditions for the γ-radiation to destroy the tumor cells [77].

The National Cancer Institute (www.nci.nih.gov) recognizes three different types of hyperthermia treatments:

1. *Local hyperthermia*: the heat is applied to a small area, such as a tumor, using various techniques that deliver energy to heat the tumor. Different types of energy may be used to apply heat; including microwave, radiofrequency, and ultrasound. The tumor site has leaky vessels allowing the NPs to enter the tumor cell by the passive targeting approach according to the particles' biophysiochemical properties. In order to increase the yield of hyperthermia, the surface of MNP is tagged by targeting molecules (i.e., active targeting) [78]. It is worth noting that there is no detectable effect on the targeting moieties (e.g., antibodies), due to the localized temperature (i.e., 42–45 °C) of the SPIONs used for hyperthermia applications [79]. The era of in vivo use of MNP for hyperthermia was initiated by Gordon et al. [80], who injected dextran coated-SPIONs intravenously into Sprague–Dawley rats and confirmed the creation of local heating in vivo.
2. *Regional hyperthermia*: large areas of tissue, such as a body cavity, organ, or limb are heated using different approaches such as external applicators or regional perfusion.
3. *Whole body hyperthermia*: is used to treat metastatic cancer that has spread throughout the body.

The modality of cancer treatment discussed in this review is a type of local hyperthermia which is called *magnetically mediated hyperthermia* or, more specifically, *magnetic fluid hyperthermia.*

Magnetic fluid hyperthermia involves dispersing magnetic particles throughout the target tissue and then applying an AC magnetic field of sufficient strength and frequency to cause the particles to heat by magnetic hysteresis losses or Néel relaxation [19,81]. Fig. 3 shows a photograph of high-frequency induction machine and its schematic representation.

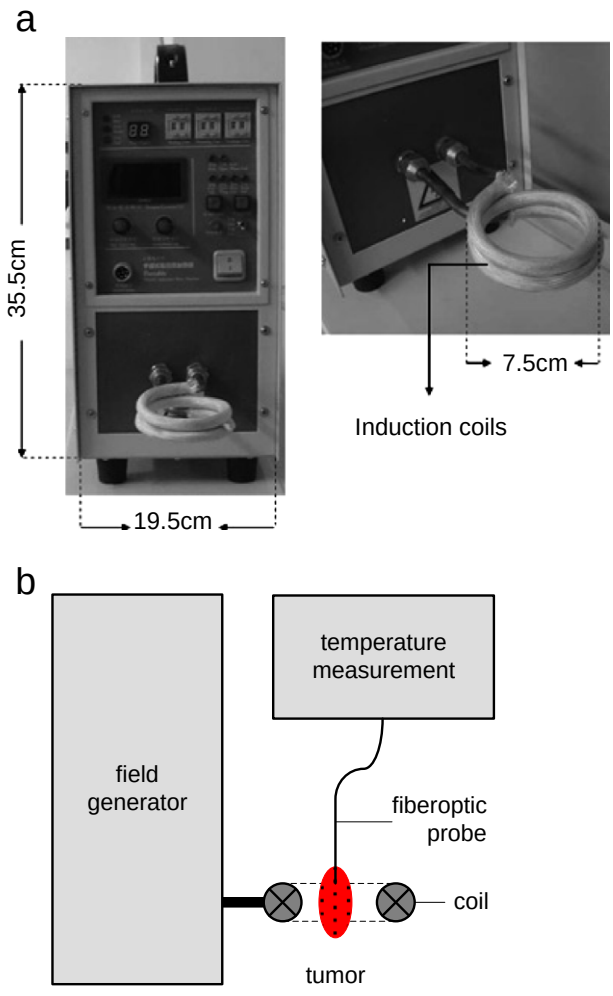

Fig. 3. (a) A photograph of the high-frequency induction machine. (b) Schematic representation induction machine, copper coils, and a temperature measurement system.
Reproduced from Ref. [82].

Among all hyperthermia modalities including microwave, laser and ultrasonic wave-based treatments, magnetic fluid hyperthermia has the best potential to selectively target the tumor cells. It might thus be possible to reduce the chemo- and radiotherapy doses despite optimizing the therapeutic effect and reducing the toxic side effects from these therapeutic modalities.

The magnetic fluid carrying the MNP is delivered in one of four ways to the tumor:

1. *Arterial injection*: the fluid carrying the magnetic particles is injected in the arterial supply of the tumor and is used as the pathway to deliver them.
2. *Direct injection*: the fluid is injected directly into the tumor. The particles will be located in the tumor tissue and the most of them in the interstitial space and a minor part in blood vessels or intracellularly [13]. Thus, when the magnetic field is applied the heat originates mostly outside the cells. Furthermore, direct injection of MNP synthesized with a coating having specific tumor antibodies is also performed [83–85] so that they are selectively ingested by the tumor cells, with minimal uptake by normal cells (differential endocytosis). This will increase the NP's retention in the tumor

region, which is desirable as the hyperthermia treatments are often done repeatedly for optimal treatment success.

3. *In situ implant formation:* injectable in situ gelling formulations are used to form gels entrapping magnetic particles into a tumor [86].
4. *Active targeting:* a more complicated way to deliver these particles to the tumor tissue is the antibody targeting [87] as well as the particle enrichment in the tumor region by an external magnetic field gradient (magnetic targeting) [88]. For antibody targeting the MNP are coated with a tumor specific antibody. After application of these MNP into the blood vessels the particles find their way to the tumor and bind there the specifically targeted receptors. Similar is the procedure of magnetically guided application of MNP. After application of the NP to the vessel an external field gradient close to the tumor tissue leads to a magnetic attraction acting on the MNP circulating in the blood stream and to their magnetic concentration in the tumor tissue. Up to now, both just described methods of active targeting are not able to provide a sufficiently high absorber concentration in the tumor for hyperthermal treatment. To use active targeting for our purposes, the efficiency of delivery has to be increased or MNP with higher specific heating power are needed.

Rosensweig [81] studied the mechanism of heat generation in a magnetic fluid due to a variable magnetic field and developed dissipation relationships based on the rotational relaxation of single-domain MNP dispersed in a liquid matrix. These particles are assumed to be less than 20 nm in diameter, so eddy current heating can be neglected. Rosensweig found that there is a strong size dependence in the heating rate [81]. The size of the particle affects the time constant of each relaxation mechanism: the larger the particles are, the larger the Brownian and Néel relaxation time constant will be. The dominating contribution will be by the faster relaxation time (see Eq. (13)).

Since hyperthermia relies on the localized heating of tumor cells to between 42 and 45 °C, high homogeneous MNP, in both size and shape, should be used [10]. In the above mentioned temperature, the normal cells would not be injured. In order to increase the safety of MNP, their uptake by normal cells could be significantly decreased using functionalization approaches (e.g., coupling to antibodies) [15,16,78,87].

The main parameter determining the heating of the tissue is the specific absorption rate (SAR); defined as the rate at which electromagnetic energy is absorbed by a unit mass of a biological material. It is expressed in Watt per kilogram and is proportional to the rate of the temperature increase ($\Delta T/\Delta t$) (Eq. (8)) for the adiabatic case:

$$SAR = 4.1868\frac{P}{m_e} = C_e\frac{dT}{dt} \tag{8}$$

where P is the electromagnetic wave power absorbed by the sample, m_e is the mass of the sample, and C_e is the specific heat capacity of the sample.

For classical high frequency irradiation by external antennas, the power deposition patterns lack selectivity. Another major difficulty in electromagnetic regional hyperthermia is the occurrence of local high temperatures (hot spots) because of the inhomogeneities of electrical permeability and conductivity of the tissue, which cause variation of the SAR [89,90].

A better control of the energy is obtained for an irradiation of the tissue doped by a ferrofluid at a low-frequency magnetic wave (100–400 kHz). For a given superparamagnetic material, the SAR is very precisely determined by the volume ratio of these crystals in the tissue. Rosensweig theoretically proved a strong relationship between the SAR of ferrofluids and its magnetic relaxation [16] (Eq. (9)):

$$SAR = 4.1868\,\pi\mu_0^2\frac{\varphi M_S^2 V}{1000kT}H_0^2\nu\frac{2\pi\nu\tau}{1+(2\pi\nu\tau)^2} \tag{9}$$

where V is the volume fraction of superparamagnetic material, ν is the frequency of the oscillating magnetic field, H_0 is the magnetic field intensity, τ is the relaxation time. Other parameters are as defined earlier.

This expression (Eq. (9)) shows that the SAR in a uniform magnetic field only depends upon the nature and the volume fraction of the superparamagnetic particles. A very high spatial selectivity can therefore be achieved if the particles are only localized in the pathological area. The irradiation frequency should be sufficiently low to avoid an interaction of the electromagnetic field with the intracellular ions, since the eddy current induced by AC magnetic field in the body may cause some damages. The strength of the eddy currents and thus an unwanted temperature increase in unloaded healthy tissue depends on the electrical conductivity of the tissue, the area exposed to the magnetic field as well as frequency and amplitude of the alternating magnetic field. In experimental investigations on volunteers Brezovic [91] found a limit for the product of H and f to be 4.85×10^8 A m^{-1} s^{-1} for a coil diameter of 0.3 m within the test person were able to "withstand the treatment for more than 1 h without major discomfort". For a different coil diameter (D) f and H can be changed in that manner that $f^*H^*D^2$ remains constant.

For small anisotropy and crystal size MNP, the SAR is proportional to the relaxation time and is due to the dissipation caused by the magnetic viscosity. It is maximum if Eq. (10) is verified.

$$\tau = \frac{1}{2\pi\nu} \tag{10}$$

For a τ longer than this optimal value, the SAR decreases very quickly because the magnetic relaxation is too slow to allow for the superparamagnetic crystal "to follow" the oscillating magnetic field. Rosensweig [81] has shown a very sharp maximum of the SAR for a diameter of about 14 nm in the case of magnetite. He has also proven that an increase of the size distribution caused a very fast decrease of the SAR. In his calculation, Rosensweig only took into account the bulk magnetocrystalline component of the anisotropy, but an evolution of the stage of aggregation of the particle should also cause a modification of the SAR because of the effect of dipolar intercrystal coupling on Néel relaxation times. This approach for localized thermotherapy induced by a magnetic fluid is already suitable for both hyperthermia and thermoablation. Evaluation of the feasibility and survival benefit of this new hyperthermia approach is in progress on animals, and clinical trials are underway [13,37–39].

The sizes of particles that could dissipate heat through Néel and Brownian relaxations of the magnetic moment have been estimated theoretically [81]. The influence of the size distribution on reversal losses is discussed theoretically mainly for ferromagnetic NP but also for particles in the transition range to superparamagnetic behavior [92]. However, the relative contribution of heat from both relaxations in materials considered for magnetic heat dissipation studies and the concept regarding the relaxation loss phenomenon suitable for practical application have not been investigated in detail but theoretical estimations show that suitable effects by Néel relaxation are only expected for optimally chosen parameters in terms of particle size, field amplitude, and frequency [93]. Fortin et al. [94] believe that the consistency between in vitro and in vivo trials is vital for the success of magnetic hyperthermia using nanosized particles. Since the heat dissipated by Brownian relaxation greatly depends on the local environment (such as viscosity of the medium), the use of magnetic particles that dissipate heat through Néel relaxation (which is not influenced by the local environment) is preferred in clinical trials. The above phenomenon has been verified recently with in vitro experiments [94] and the importance of a detailed analysis of the relative contribution for effective therapy has been stressed more than ever before.

Another factor that retards the progress of magnetic hyperthermia is related to the expression used to denote the potential of the thermal seeds. There have been several reports on heat dissipation of magnetite particles exposed to various magnetic field strengths and frequencies [16,95–98], and a SAR value as high as 960 W g^{-1} has been reported at 410 kHz and field amplitude 10 kA/m in magnetosomes [99]. However, it should be noted that the present practice of reporting the SAR values in W g^{-1} does not fully express the true potential of thermal seeds because heat dissipation is proportional to the frequency and square of the magnetic field strength used during the measurements. Thus, it is difficult to arrive at any conclusion regarding the physical properties of magnetite suitable for effective hyperthermia, unless the magnitudes of magnetic field strength and frequency are considered. In spite of the above problems, researchers have gone another step forward in treating human patients with brain and prostate cancer using a magnetic fluid suspension dispersing magnetite [25,35]. It should be noted that for effective magnetic fluid hyperthermia (MFH) treatment, it is vital to continue research in the fields of (i) synthesis of monodispersed magnetic particles, (ii) heat dissipation characteristics of magnetite particles, and (iii) heat diffusion characteristics, so that the concentration of thermal seeds necessary to elevate the temperature above 43 °C and the temperature distribution in the tumor vicinity can be optimized.

4. Heat dissipation mechanism

Heat dissipation from magnetic particles is caused by the delay in the relaxation of the magnetic moment through either the rotation within the particle (Néel) or the rotation of the particle itself (Brownian), when they are exposed to an AC magnetic field with magnetic field reversal times shorter than the magnetic relaxation times of the particles. The Néel (τ_N) and Brownian (τ_B) magnetic relaxation times of a particle are given by the following equations (Eqs. (11)–(13)):

$$\tau_N = \tau_o e^{\frac{KV_M}{kT}} \tag{11}$$

$$\tau_B = \frac{3nV_H}{kT} \tag{12}$$

$$\tau = \frac{\tau_B \tau_N}{\tau_B + \tau_N} \tag{13}$$

where τ_N is the Néel relaxation time, τ_B the Brown relaxation time, τ the effective relaxation time if both effects occur at the same time, $\tau_0 = 10^{-9}$ s, K the anisotropy constant, V_M the volume of particle, k the Boltzmann constant, T the temperature, η the viscosity, and V_H the hydrodynamic volume of particle.

From the above equations, it is clear that the relaxation time relies on the particle diameter. When the particles are exposed to an AC magnetic field with time of magnetic reversals less than the magnetic relaxation times of particles, heat is dissipated due to the delay in the relaxation of the magnetic moment. Thus, the heat dissipation value is calculated using the harmonic average of both relaxations and their relative contributions depending on the particle diameter. The heat dissipation is given by the following equation (Eq. (14)):

$$P = \mu_0 \chi'' f H^2 \tag{14}$$

where P is the heat dissipation value, μ_0 the magnetic field constant, χ'' the AC magnetic susceptibility (imaginary part), f the frequency of the applied AC magnetic field, and H the strength of the applied AC magnetic field.

A theoretical estimation of the SAR values as a function of particle diameter (up to the superparamagnetic size limit) can be calculated using Eq. (14). The heat dissipated through Néel relaxation is not influenced by the viscosity of the medium; whereas, the Brownian relaxation is greatly influenced. For example, if the viscosity of the medium is high or if the freedom of particle rotation is suppressed, the heat dissipated by these particles will either diminish or seize. Thus, to obtain similar SAR values in in vitro and in vivo experiments; it is essential to have particles that relax through Néel relaxation. Therefore, it is always necessary to determine the relative contribution of heat from Néel and Brownian relaxation losses to estimate the possible minimum and maximum heat that could be generated in in vivo experiments.

An attempt has been made to determine the relative contribution from magnetite samples of two different suspensions with average diameters of 12.5 and 15.7 nm. Heating characteristics depended on the dispersion states of particles. The specific absorption rates (SAR) dropped by 27% for the 12.5 nm particles to 16.8×10^{-9} W g^{-1} Oe^{-2} Hz^{-1} and by 67% for the 15.7 nm particles to 9.69×10^{-9} W g^{-1} Oe^{-2} Hz^{-1}, when the particle rotation was suppressed by dispersing MNP in hydrogel [100].

SPIONs can produce heat by the loss mechanism which is obtained from the rotation of magnetic moments in overcoming the energy barrier. Energy is generated by the relaxation of the MNP′ moment to its equilibrium orientation (i.e., Néel relaxation) [101]. Per definition hysteresis is zero for superparamagnetic materials. But in real SPIONs ensembles, a hysteresis loop with a negligible remanence and coercivity occurs [102] probably due to some large particles and agglomerates in the ensemble.

In addition to SPIONs, particles that show hysteresis might also be interesting for hyperthermia [101]. These particles can be ferrimagnetic (larger single cores above the superparamagnetic size limit) [103] or superferromagnetic (clusters of superparamagnetic cores which show ferromagnetic behavior due to magnetic interactions of the single cores) [104]. When assuming a relative strong immobilization of these larger particles (15 to 25 nm for the ferrimagnetic MNP, up to 100 nm for the superferromagnetic cluster) in the tumor tissue after application [105] a reversal of the magnetization is possible neither by Néel nor Brown relaxation. By applying an alternating field with amplitude of more than 2 times of the coercivity of the particles the hysteresis will be overcome and the flipping of the magnetization in the particles leads to heating of the particles. Typical values for SAR for this magnetic hysteresis heating are in the range from 100 to 800 W/g.

Superparamagnetic MNP show medium heating efficiency, but it can be enhanced by increasing their sizes [106]. It is worth noting that heating efficiency is crucial for clinical purposes, given that it makes it possible to minimize the patient's complaints (e.g., the injected dosage is decreased by enhancing the produced heat per NP) [101]. Furthermore the heating efficiency of the MNP is crucial for the size of tumors which can be heated up. Due to the higher surface-to-volume ratio of smaller tumors a stronger heat dissipation to the surrounding tissue takes place [19,107]. This means that for very small tumors a high specific absorption rate or a high concentration of absorbing material in the tissue is needed. For the direct injection a concentration of 10 to 100 mg particles per cm [3] of tumor tissue is realistic. Thus, for the treatment of single cells or cell clusters it seems unrealistic to reach a sufficient temperature increase with the available groups of MNP and the achievable MNP concentrations (see Fig. 4) [108].

5. Magnetic materials used for thermotherapy and their magnetic properties

There are several magnetic nanomaterials that have been used in hyperthermia applications including SPIONs (Fe_3O_4 and γ-Fe_2O_3), iron–palladium and cobalt, ferrimagnetic spinels, cobalt ferrite, Mn–Zn and Mn–Zn–Gd ferrite particles, copper–nickel, ferromagnetic perovskites $La_{1-x}Sr_xMnO_3$, $Ni_{(1-x)}Cr_x$, gadolinium-, calcium-, and

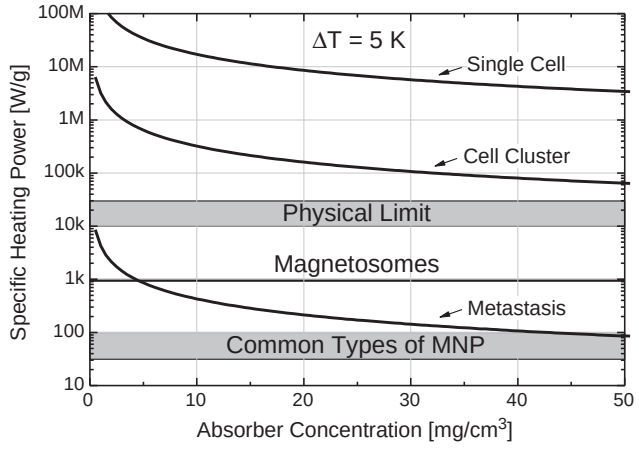

Fig. 4. Specific loss power needed for hyperthermia ($\Delta T = 5$ K) in dependence on particle concentration achieved in tumor tissue. Given are curves for metastases of 3 mm diameter, a cell cluster (0.1 mm) and a single cell (15 μm).

lanthanum complexes, and ferrimagnetic $SrFe_{12}O_{19}$/γ-Fe_2O_3 composites [1,45,101,109–119].

There is another novel method/idea to control the heating between 42 and 45 °C (hyperthermia) or over 46 °C (thermo-ablation that damages cells irreversibly). In this method, a new class of magnetic materials (e.g., Mn–Zn–Fe, Co–Gd–Zn, and Zn–Gd–Fe composites) has a Curie temperature (i.e., the temperature above which the ferromagnetic materials lose their strongly magnetic properties and become paramagnetic) which is just above the therapeutic temperature. The heating would then decreased considerably once the desired therapeutic temperature is exceeded, and no charring of the tissue would be possible. First such materials were described in 1999 [115,120] and the useful temperatures have slowly been coming down [121,122]. Most recently, Settecase et al. [123] prepared MNP with a Curie temperature of 42–43 °C and employed the MNP as selective heating source for a tumor site exposed to an alternating magnetic field.

By modifying their synthesis parameters (e.g., doping of the guest atom in the structure [124]), and their physiochemical properties (e.g., composition, structure, shape, size and its distribution), the magnetic properties of MNP could be significantly changed. For instance, the structure of ferrimagnetic NPs (e.g., $Co_xFe_{1-x})_{\text{tetrahedral site}}[Co_{1-x}Fe_{1+x}]_{\text{octahedral site}}O_4$; $0.07 \le x \le 0.2$) and consequently their magnetic properties (e.g., magnetic saturation and magnetocrystalline anisotropy constant) could be changed by variation of quenching speeds [110,125]. In order to control the coercivity, remanence and, consequently, the shape of the hysteresis loop, multiphase materials have been designed such as $SrFe_{12}O_{19}$/γ-Fe_2O_3 composites. These materials have different magnetic properties from each phase; in addition, the ratio of various phases is crucial for the prediction of obtained magnetic properties [126].

6. The importance of SPIONs for hyperthermia

Although SPIONs exhibit a medium heating efficiency with minimal control of in vivo temperature evolution during hyperthermia in comparison with other magnetic materials [101], it is surprising to note that most of both experimental and commercially available MNP for hyperthermia applications consist of SPION cores rather than other mentioned MNP (see www.magforce.de and www.sennewald.de, the most eminent companies in hyperthermia). The reason is that the MNP must have many characteristics to qualify for biomedical applications such as biocompatibility, nontoxicity, ability to escape from the reticuloendothelial system (RES), and low protein adsorption [127,128]. In addition, the integrative therapeutic and diagnostic (i.e., theragnostic) capacity is of crucial importance in nanomedicine in order to reduce side effects in patients [78,129]. Due to their capability to be functionalized and guided by a magnetic field, and their biocompatibility and theragnostic potential, SPIONs represent a cutting-edge tool for nanomedicine (the most popular systems are presented in Table 1) [1,102,130–135]. SPIONs can simultaneously satisfy many biomedical needs and are for this reason used in magnetic resonance imaging, guided drug/biomolecules delivery, magnetic hyperthermia, and tissue repair without any detectable cytotoxicity at the applied dosage [1,136–139].

The cytotoxicity of SPIONs, at concentrations of several hundred times of the applied dosage, has been tested via various methods such as the cell-life cycle assay, MTT assay, comet assay, TUNEL assay (i.e., for apoptosis detection). No considerable toxicity was found [78,102,127,128,130–137,139–141], whereas other magnetic particles have shown considerable toxicity in the same dosage [141–144]. One type of SPIONs for imaging applications has been approved by the FDA and is already on the market [145].

Superparamagnetic MNP are preferred in in vivo applications, as the magnetization disappears once the external magnetic field is removed. It is notable that superparamagnetism is a phenomenon which is observed in ferromagnetic nanoparticles below a critical size to form single domain particles. The main characteristic of this form of magnetism is that these particles do not show any magnetization in the absence of a magnetic field. Particle agglomeration, and hence the

Table 1
Most popular magnetic particle systems in hyperthermia.

Type of system	Example of treated-cells/tumors	Remarks	References
Core–shell system	Several human carcinoma cell lines. Several in vivo examinations	Passive targeting system commonly used for local treatment with low targeting capability.	[14,147–149]
		Active system commonly used for local treatment with high targeting capability.	[150–152]
		Using pH- and thermo-sensitive polymers, the system could be used as a controlled delivery system as well. The therapeutic yield, in comparison with the conventional methods (e.g., surgery, chemotherapy, radiation, and immunotherapy) is significantly increased; on/off control over release rates is possible.	[153–158]
Magnetoliposomes; encapsulated SPIONs in the liposomal shell	Rat glioma cells; T-9 rat glioma; B16 mouse melanoma; Os515 hamster osteosarcoma; VX-7 squamous cell carcinoma in rabbit tongue; mouse renal cell carcinoma	The blood circulation time has been increased in comparison with SPIONs themselves.	[159–163]
		Targeting moieties could significantly enhance the treatment yield.	[164,165]
Magnetic microspheres/microcapsules	Several in vivo investigations	The blood circulation time is increased; the system has the potential to be used in theragnostic applications (hyperthermia, imaging, and drug delivery).	[166–168]

possible embolization of the capillary vessels, can thus be avoided [2,146].

Although the hysteresis loop of ferrimagnetic and ferromagnetic NPs is advantageous for hyperthermia, its existence might induce embolization of the capillary vessels due to the formation of agglomerates, which limits their in vivo use. It is worth mentioning that the heat induction in SPIONs can be enhanced by the creation of magnetic microspheres which consist of a polymer matrix randomly filled with MNP [102,133]. This enhancement of the local heating of SPIONs in magnetic microspheres may relate to the magneto-crystalline anisotropy [133]. Since the SPIONs in the microspheres cannot move to their easy axes directions, the inserted energy is transferred into heat.

7. Effect of dopants on the enhancement of the hyperthermic properties of SPIONs

By enhancing the magnetic characteristics, the hyperthermia output of SPIONs can be significantly increased [169]. There are several ways for improving the magnetic properties of MNP, such as the unidirectional growth of MNP [140], metal dopant substitution strategy of metal ferrite NPs [170,171], and the formation of colloidal nano-crystal clusters [172,173]. Among the mentioned methods, using a metal dopant such as Zn and Gd in SPIONs has shown a better enhancement of magnetic properties [140,174–176].

An example for metal dopant substitution therapy is the use of Gd-doped SPIONs ($Gd_{0.02}Fe_{2.98}O_4$) which were prepared by Drake et al. The specific power adsorption rate was about 4 times higher than the one of identically sized SPIONs [176]. The obtained doped-SPIONs were employed in mouse for in vivo tumor thermo-therapy and the results confirmed their ability to inhibit tumor growth in comparison with standard SPIONs. One technical problem with metal-doped MNP, however, is the difficulty of producing them in a reliable and reproducible fashion [177]. Jang et al. [169] achieved the dopant's proper positioning in tetrahedral sites as well as the scale up capability. In addition, their doped-SPIONs showed very high saturation magnetization (175 emu/g) and the largest MRI contrast effects in comparison with the other available contrast agents. According to the results, the doped-SPIONs have an eight- to fourteen-fold increase in MRI contrast and a fourfold enhancement in hyperthermic effects compared to the conventional SPIONs (see Fig. 5) [169].

8. Temperature mapping in vivo

In order to optimize the treatment procedure while at the same time minimizing the effects of hyperthermia treatment to normal cells/tissues, temperature mapping at the treatment site is recognized as crucial. Modern methods of temperature mapping include the use of magnetically insensitive fiber-optic probes at a variable magnetic field [178], thermochromic fluorescent- and optical-films [179], MRI thermometry [180], imaging by superconducting quantum interference sensors [181], and molecular diffusion by functional-MRI [182]. In addition, a better understanding of hyperthermia and its heat distribution in vivo is achieved by hybrid thermal mapping of tumors using the combination of for example optical and MR imaging, and CT [114].

Recently, the Magforce Company introduced a very useful, precise and functional software platform therapy planning system (with the commercial name of NanoPlan®), which is a new thermal solver with an explicit temperature gradient formulation based on finite differences [79]. This gradient formulation can calculate the heat flow on thermal limiting surfaces with any desired shape. In addition, the employed thermal solver has the capability to establish time-dynamic 3D temperature distributions in any desired voxel constellations of a thermally non-homogeneous medium. Hence, the estimation time of thermotherapy with the assessment of the risks in the stage of the temperature elevation can be defined [79]. Several studies employed NanoPlan® to calculate the expected temperature distribution within the treatment area for a desired magnetic field strength [35,38]. The modeling data agreed very well with the experimentally obtained measurements. Another company, Dr. Sennewald Medizintechnik GmbH, has developed a similar software, SigmaHyperPlan® [183].

A clinical trial that employed NanoPlan® for in vivo temperature mapping, temperature distribution calculations and visualizations in the treatment area in relation to H (magnetic field) and the underlying SPION distribution (see Fig. 6) was performed by Wust et al. [38]. They used aminosilane coated-SPIONs (prepared by MagForce Nanotechnologies AG, Berlin, Germany) on twenty-two patients with non-resectable and pre-treated solitary tumors. The coated-SPIONs, with an average core-size of 15 nm, were dispersed in water with an iron concentration of 112 mg/mL. By employing the tolerable H-field-strengths of 3.0–6.0 kA/m in the pelvis, up to 7.5 kA/m in the thoracic and neck region, and >10.0 kA/m for the head, SAR values of 60–380 W/kg in the target were obtained leading to a 40 °C heat-coverage of 86%. According to the results of the actual nanoparticle distribution and derived temperatures, the authors claimed that a moderate increase of the H-field, by even just 2 kA/m, would significantly improve the 42 °C coverage towards 100% [38].

9. Biocompatibility of SPIONs

Given their novel physiochemical properties, there are great hopes for the development of new theragnostic possibilities in medicine based on SPIONs. However, in order to be used for safe and high yield biomedical applications, SPIONs must be coated by materials that satisfy the following requirements: (i) preventing the opsonization of SPIONs, which leads to the fast removal of the particles from the blood stream by the RES; (ii) avoiding agglomeration of SPIONs in biological medium; (iii) achieving the desired surface charge for the SPIONs' main task; (iv) preserving the functionalities of the nanomaterials; (v) exhibiting the protein absorption on the SPIONs' surface and their corresponding denaturation; and (vi) ensuring the biocompatibility of the SPIONs [78,127,130,138]. In order to achieve these requirements, several organic and inorganic coatings have been employed on the surface of SPIONs. These coatings include polyethylene glycol [184], polyethylene glycol fumarate [133], polyvinyl alcohol [132], acrylate-based coatings [164,185], polysaccharide-based coatings [166,186], synthetic polyesters [187,188], alginate [189], chitosan and polyethylenimine [190–194], gold [195], and silica [196]. Cytotoxicity of the bare and coated SPIONs has been assessed via various methods, such as the MTT (3-(4,5-dimethylthiazol-2-yl)-2,5-diphenyltetrazolium bromide) assay [133], the comet assay [141], the cell-life cycle assay [137], the TUNEL assay [131], and several in vivo models [130,161,197,198]. The results confirm the biocompatibility of both bare and coated SPIONs at the applied doses, which were much higher than currently approved dose (i.e., 0.56 mg/kg) in humans [199].

10. Determination of physiochemical properties of SPIONs

The magnetic properties of MNP depend on their size, shape and microstructure. Several techniques can be used to determine their size and chemical composition and the properties of their magnetic surface. The size of the particles can be determined by transmission electron microscopy (TEM) images. This technique reports the total particle size and provides details of the size distribution. X-ray diffraction (XRD) can be performed to obtain information on the crystalline structure of the particles. The crystal size can be calculated also from the line broadening of the XRD pattern using the Scherrer formula. Mössbauer spectroscopy is an alternative technique for assessing crystal composition. This method gives information about the order of magnitude of the Néel relaxation time, an important characteristic of superparamagnetic particles. The photon correlation

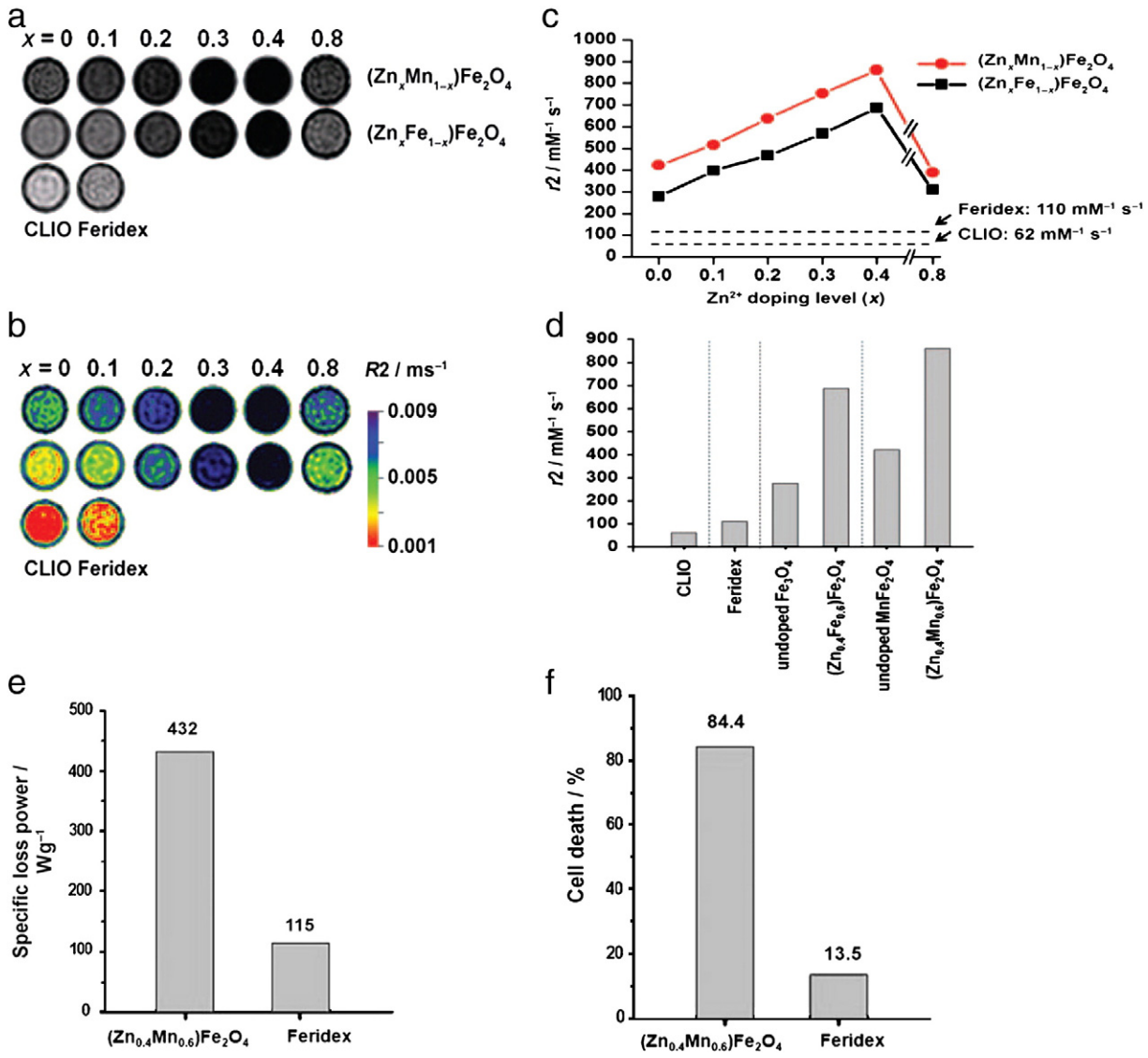

Fig. 5. MR contrast effects of $(Zn_xFe^{2+}{}_{1-x})Fe_2O_4$ NPs (Zn-doped SPIONs) upon changes in the Zn^{2+} doping level (i.e., x) for (a) T_2-weighted MR images of $(Zn_xFe^{2+}{}_{1-x})Fe_2O_4$ NPs, and commercial SPIONs (i.e. Feridex and cross-linked iron oxide (CLIO)), and (b) their color-coded images, where red indicates low R_2 and violet indicates high R_2 values; (c) Graphs of r_2 versus Zn-doped SPIONs at 4.5 T; (d) Comparison of r_2 values of MNP, showing that Zn-doped SPIONs have considerably improved MRI contrast effects in comparison with commercial SPIONs; (e) Specific loss power values for $(Zn_{0.4}Fe^{2+}{}_{0.6})Fe_2O_4$ and Feridex in a 500 kHz AC magnetic field with an amplitude of 3.7 kA/m; (f) Percentage of Zn-doped SPIONs- and Feridex-treated HeLa cells which after subsequent application of an AC magnetic field for 10 min.
Reproduced with permission from Ref. [169].

spectroscopy (PCS) measurement gives a mean value of the hydrodynamic diameter of the particles. Magnetometry confirms the superparamagnetic properties of the particle and provides information on the specific magnetization and the mean diameter of the crystals. The fitting of the nuclear magnetic resonance dispersion (NMRD) curves according to the relevant theories gives the mean crystal size, the specific magnetization, and the Néel relaxation time [1,200].

11. Smart systems for multi-purpose bio-applications

Smart systems consist of a magnetic core for heat production and a multi-stimuli sensitive shell, such as pH- and thermo-sensitive polymers (e.g., block copolymers and copolymer hydrogels) [201]. These systems could significantly improve therapies for diseases. The localized and triggered treatments have emerged to enhance the hyperthermia treatment potential by delivering drugs to the targeted sites [153]. The drug is loaded in the stimulus sensitive shell, as enteric coatings to protect the release of drug. Upon reaching the targeted site, the temperature of magnetic core is increased (e.g., by an alternating current magnetic field) leading to the structural/conformational changes (e.g., breaking of covalent or non-covalent chemical bonds) in the thermo-sensitive polymeric shell. Consequently, the drug is released locally in the cancerous site [153,202,203] (Fig. 7). Similarly, not only thermo-sensitive properties, but also pH-sensitive characteristics of polymers can be utilized to target inflammatory sites [201]. The commonly known multi-stimuli responsive polymers are presented in Table 2. Their main application is the specific drug release. More information considering these polymers can be found in several comprehensive reviews [201,204–208].

In order to have a good control of the release profile, the amount of heat produced by the magnetic core should be optimized. It is noteworthy that in the optimization process, a good knowledge of the several relevant factors should be achieved (e.g., the strength and frequency of the applied magnetic field, the depth and concentration of the smart MNP in tissue, their size, shape and composition) [81,209]. In

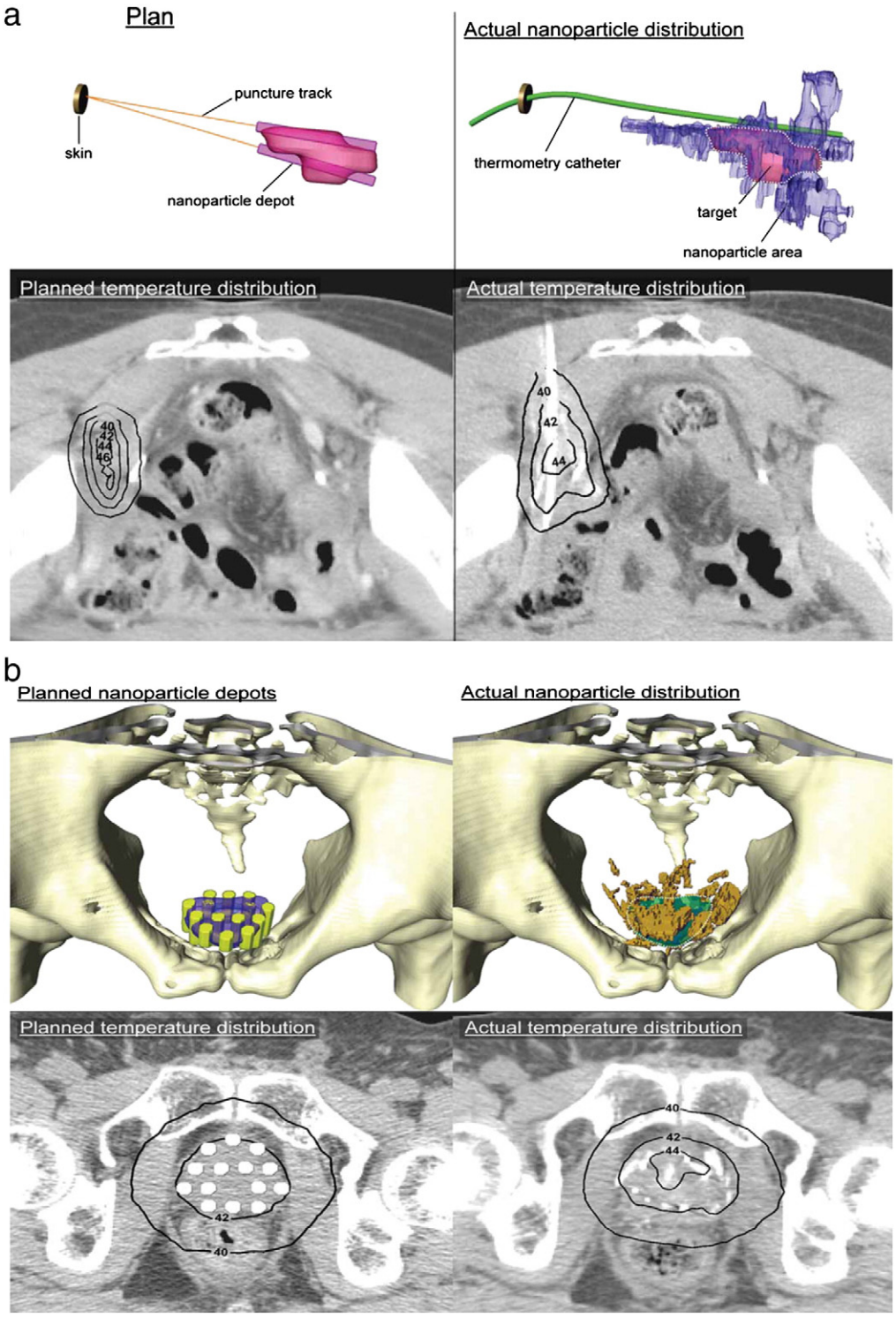

Fig. 6. Comparison of the NanoPlan®-predicted and actual SPION- and temperature distribution for (a) recurrent cervical cancer of the pelvic wall and (b) recurrent prostate carcinoma.
With permission from [38].

addition to thermo-sensitive properties, some polymeric shells (e.g., polyethylene glycol based hydrogels) have a cross linking capability that leads to more controlled delivery systems [133,210].

Hayashi et al. [230] showed that heat is not only useful for hyperthermia treatment, but also can act as a driving force for drug-release. In this case, β-cyclodextrin (CD) acted as a drug container for hydrophilic (paclitaxel) or lipophilic (doxorubicin) structures. Drugs incorporated in the CD can thus be released through the use of induction heating, or hyperthermic effects, by applying a high-frequency magnetic field. For example, Hayashi et al. [228] synthesized folic acid (FA) and CD-functionalized SPIONs, FA-CD-SPIONs; FA being well-known as a targeting ligand for breast cancer tumor and endowing the SPIONs with a cancer-targeting capability. Through induction heating, drug release was triggered from the CD cavity on the particle—a behavior that was controlled by switching the high-frequency magnetic field on and off. The FA-CD-SPIONs are no

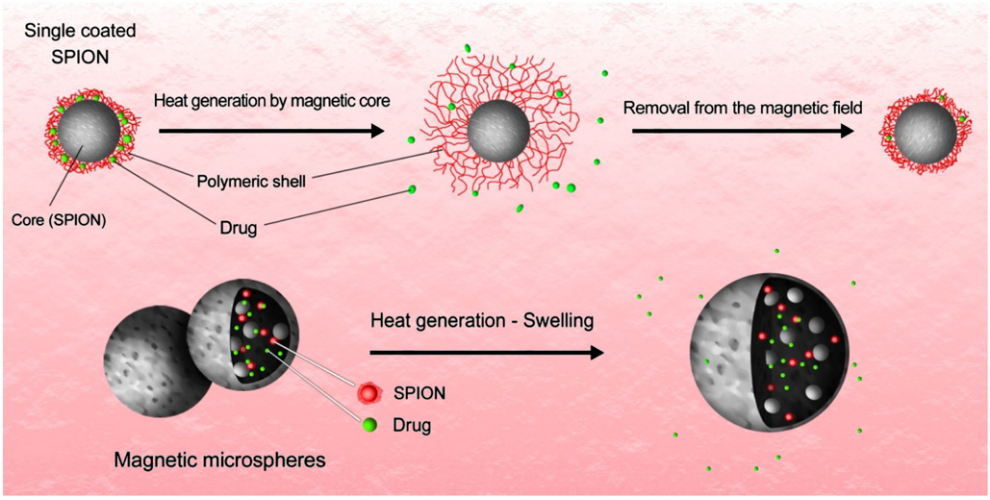

Fig. 7. Popular multi-purpose systems in hyperthermia and drug delivery.

cytotoxic for cells. Thus, these systems can serve as a novel device for performing drug delivery and hyperthermia simultaneously.

Another drug delivery system, based on covalently attaching genistein onto Fe_3O_4 MNP coated by cross-linked carboxymethylated chitosan (CMCH), has been developed [231]. The effects of free genistein and Fe_3O_4-CMCH-genistein nanoconjugate on the proliferation and apoptosis of the gastric cancer cell line SGC-7901 were investigated by MTT assay and flow cytometry (FACS). Together, these methods indicated that the Fe_3O_4-CMCH-genistein nanosystem significantly enhanced SGC-7901 cancer cell apoptosis. This drug delivery system is thus promising for future multifunctional chemotherapeutic applications that combine drug release and magnetic hyperthermia therapy [232].

12. Examples of in vivo applications

The influence of biomagnetic Fe/Fe_3O_4 core/shell MNP combined with short external alternating magnetic field (AMF) exposure on the growth of subcutaneous mouse melanomas (B16-F10) was evaluated [150]. These MNP were designed for cancer targeting after intratumoral or intravenous administration. The magnetic hyperthermia results obtained after intratumoral injection indicated that micromolar concentrations of iron given within the modified MNP caused a significant anti-tumor effect on murine B16-F10 melanoma with three short 10-minute AMF exposures. A decrease in tumor size was also observed after intravenous administration of the MNP followed by three consecutive days of AMF exposure 24 h after the MNP injection. These results indicate that intratumoral administration of surface modified MNP can attenuate mouse melanoma after AMF exposure. Moreover, the authors found that after intravenous administration of micromolar concentrations, these MNP were capable of causing an anti-tumor effect in a mouse melanoma model after only a short AMF exposure time. In this case, the tumors decreased compared to the control group which increased.

Matsuoka et al. [162] have developed magnetic cationic liposomes (MCL) based on SPIONs and investigated their in vivo efficacy for hyperthermia treatment of hamster osteosarcoma. Magnetoliposomes were injected directly into the osteosarcoma and then subjected to an alternating magnetic field. The tumor was heated above 42 °C, and complete regression was observed in 100% of the treated group hamsters (Fig. 8). At day 12, the average tumor volume of the treated hamsters was about 1/1000 of that of the control hamsters.

Du et al. [233] assessed the thermodynamic characteristics of a nanosized As_2O_3/Fe_3O_4 complex and validated the hyperthermia effect, when combined with magnetic fluid hyperthermia (MFH), on xenograft HeLa cells (human cervical cancer cell line) in nude mice. Thermo chemotherapy with these MNP showed a significant inhibitory effect on the mass (88.21%) and volume (91.57%) of xenograft cervical tumors ($p<0.05$ for each measurement). In addition, the expression of CD44v6, VEGF-C, and MMP-9 mRNA, which are related to cancer and/or metastasis, were significantly inhibited. These nanosystems combined with MFH are thus a promising technique for the minimally invasive elimination of solid tumors and may also be useful for the treatment of metastases by inhibiting the expression of several growth-related factors.

A feedback temperature control system has been developed to keep the MNP at a constant temperature to prevent overheating in the tumors such that a safer and more precise cancer therapy becomes feasible [234]. The technique involves injecting a formulation that solidifies and form an implant in vitro. The implant entraps SPIONs embedded in silica microbeads to magnetically induce hyperthermia, and it can be repeatedly heated in an AMF. By using the feedback

Table 2
Common polymers showing thermo-sensitive characteristics.

Shell		Remark	References
Poly(N-isopropylacrylamide)		Lower critical solution temperature (LCST) of 40–45 °C; LCST can be altered by the judicious selection of co-monomers that impart an increase or decrease in the polymer's hydrophilicity; squeezing-controlled release is the main drug releasing mechanism.	[201,211–216]
Poly(N,N′-diethylacrylamide)			[217–219]
Poly(propylene oxide)			[220–222]
Poly(vinyl ethers)			[223,224]
Copolymers	Poly(methacrylic acid-co-N-isopropylacrylamide)	Both thermo- and pH-sensitive properties	[225–227]
	Poly(N-isopropylacrylamide-co-N-acryloylpyrrolidine)	Two step thermally induced aggregation in water	[228]
	Poly(ethoxyethyl glycidyl ether)/poly(propylene oxide) triblock	Two thermo-sensitive blocks have LCST properties	[229]

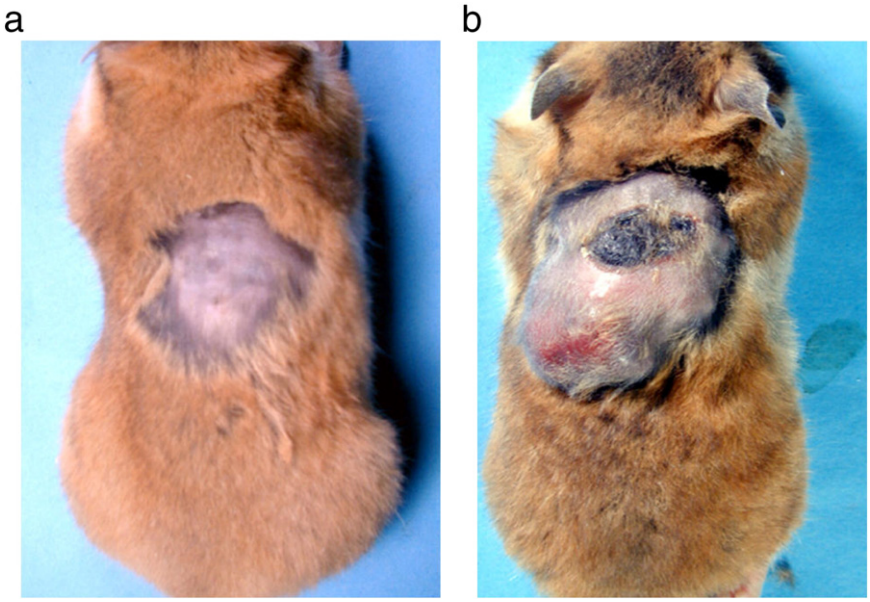

Fig. 8. Typical photographs of hamsters on day 20 after injection with 0.4 mL of the cationic magnetoliposomes (net magnetite weight 3 mg). (A) Treatment group. (B) Control animals without AMF treatment.
With permission from [162].

temperature control system, MNP can be heated up to specific constant temperatures, e.g., 37, 40, 42, 45, 46, and 47 °C, with a variation of less than 0.2 °C. With this approach, the in-vitro survival rate of tumor cells at different temperatures can be systematically explored. The authors found experimentally that the survival rate of cancer cells could be greatly reduced when CT-26 cancer cells were heated above 45 °C. In addition, localized temperature increases as high as 59.5 °C could be successfully generated in rat livers. Finally, they report that a complete regression of the tumor was achieved.

Le Renard et al. [82] investigated a new heat delivery technique for the local treatment of solid tumors. Their technique involves injecting a formulation that solidifies to form an implant in situ. This implant entraps SPIONs embedded in silica microbeads for magnetically induced moderate hyperthermia. Particle entrapment prevents phagocytosis and distant migration of SPIONs. They evaluated heating and treatment efficacies by means of thermometry and survival studies in nude mice carrying subcutaneous human colocarcinomas. After injection of the formulation into the tumor, a single 20 min hyperthermia treatment was delivered by 141 kHz magnetic induction using field strengths of 9 to 12 mT under thermometry. After treatment with the 12 mT field, five of eleven mice (45%) survived 1 year without any tumor recurrence; a result that is promising for tumor therapy using magnetically induced moderate hyperthermia through injectable implants.

The efficiency of thermotherapy using magnetic nanoparticles for minimally invasive treatment was investigated on experimental glioblastoma multiforme in a rat tumor model [24]. Tumors were induced by implantation of RG-2-cells into the brains of rats. Treatment was carried out using an alternative magnetic field system operating at a frequency of 100 kHz and variable field strength of 0–18 kA/m. The effectiveness of treatment was investigated by the survival time of the animals and histopathological examinations of the brain and the tumor. Thermotherapy with aminosilane-coated nanoparticles led up to 4.5-fold prolongation of survival over controls.

Recently, Bruners et al. [235] showed that CT-guided magnetic thermoablation of malignant kidney tumors is technically feasible in an animal model. Tumors were implanted into the kidneys of rabbits and allowed to grow for 2 weeks. After preinterventional CT perfusion imaging, CT-guided injection of MNP was performed, followed by exposure of the animals to an alternating electromagnetic field for 15 min ($\approx$0.32 kA/m). Then animals underwent CT perfusion imaging again. After image-guided intratumoral injection of ferrofluids, the depiction of nanoparticle distribution by CT correlated well with macroscopic evaluation of the dissected kidneys.

13. Conclusions and future perspectives

SPIONs play an important role in the development of hyperthermia for treatment of tumors in vivo. Size and surface modified MNP enable a safe application to the tumor and high heating efficiency by Neel relaxation which promises good therapeutic success. Grafting cancer-specific binding agents to MNP would make magnetic fluid hyperthermia treatment much more selective than traditional chemotherapy and even conventional hyperthermia. Furthermore, MNP can be magnetically targeted and/or concentrated in the target tissue, and heating is then only induced to significant temperatures where the MNP have been deposited. In addition, tissue-deposited MNP will generally stay where they were initially deposited, thus allowing for repeated and concentrated hyperthermia treatments in the same area.

At the moment the amount of particles delivered to the tumor tissue by means of antibody targeting is too low for a sufficient temperature increase. Therefore, the challenges in this field will be the design of stealth nanoparticles able to circulate in the blood compartment for a long time and the surface grafting of ligands able to facilitate their specific internalization in tumor cells. Many groups focus their work on the development of improvement of these targeting so that an enhancement of the targeting efficiency can be expected in the near future. The absorber concentrations reachable in a tumor by direct injection are able to produce enough heating power with present particles for hyperthermia treatment. But for the use of antibody targeted SPIONSs the heating power of the particles has to be increased. This improvement can be reached by optimized combination of particle diameter and size distribution with the amplitude and frequency of the alternating magnetic field.

Most research has been evaluated in preclinical studies. The results of first clinical trials are very promising. But it is too early to claim therapeutic advantages because survival and disease progression benefits were not defined endpoints of the feasibility studies.

There are several matters that should be considered to enhance the hyperthermia yield of SPIONs, such as in vivo control of heat distribution [236], managing of the nanoparticles' surface for fast internalization by the target cells [237], and optimization of the biophysicochemical properties [238]. An inhomogeneous particle distribution in the tissue may lead to the occurrence of hot spots where the high temperature causes necrosis of the tissue. In contrast, in regions with a low particle concentration the temperature is not sufficient high to trigger the onset of apoptosis and proliferation of surviving tumor cells [239] can appear. Both effects should be prevented and thus methods for a homogeneous placement of particles in the tissue as well as the monitoring of the spatial heat distribution must be integral parts of future research.

Finally, it can be said that it is worth noting that great efforts have led to promising preclinical and clinical trials of magnetic hyperthermia by using water based dispersions containing SPIONs. From the physical point of view SPIONs are very suitable to serve as heating source during magnetic fluid hyperthermia and further research in this field will lead to a feasible solution or reduction of the above mentioned problems which enables a more profound testing of this promising therapeutic method for cancer treatment.

References

[1] Laurent S, Forge D, Port M, Roch A, Robic C, Vander Elst L, et al. Magnetic iron oxide nanoparticles: synthesis, stabilization, vectorization, physicochemical characterizations and biological applications. Chem Rev 2008;108(6):2064–110.
[2] Mornet S, Vasseur S, Grasset F, Duguet E. Magnetic nanoparticle design for medical diagnosis and therapy. J Mater Chem 2004;14:2161–4.
[3] Katz E, Willner I. Integrated nanoparticle-biomolecule hybrid systems: synthesis, properties, and applications. Angew Chem Int Ed 2004;43(45):6042–108.
[4] Matsunaga T, Okamura Y, Tanaka T. Biotechnological application of nano-scale engineered bacterial magnetic particles. J Mater Chem 2004;14(14):2099–105.
[5] Park J, An K, Hwang Y, Park JEG, Noh HJ, Kim JY, et al. Ultra-large-scale syntheses of monodisperse nanocrystals. Nat Mater 2004;3(12):891–5.
[6] Song Q, Zhang ZJ. Shape control and associated magnetic properties of spinel cobalt ferrite nanocrystals. J Am Chem Soc 2004;126(19):6164–8.
[7] Sun S, Zeng H, Robinson DB, Raoux S, Rice PM, Wang SX, et al. Monodisperse MFe_2O_4 (M = Fe, Co, Mn) nanoparticles. J Am Chem Soc 2004;126(1):273–9.
[8] Tartaj P, Serna CJ. Synthesis of monodisperse superparamagnetic Fe/silica nanospherical composites. J Am Chem Soc 2003;125(51):15754–5.
[9] Lyon JL, Fleming DA, Stone MB, Schiffer P, Williams ME. Synthesis of Fe oxide core/Au shell nanoparticles by iterative hydroxylamine seeding. Nano Lett 2004;4(4):719–23.
[10] Pankhurst QA, Connolly J, Jones SK, Dobson J. Applications of magnetic nanoparticles in biomedicine. J Phys D Appl Phys 2003;36(13):R167–81.
[11] Gubin SP, Koksharov YA, Khomutov GB, Yurkov GY. Magnetic nanoparticles: preparation, structure and properties. Russ Chem Rev 2005;74(6):489–520.
[12] Gilchrist RK, Shorey WD, Hanselman RC, Parrott JC, Taylor CB. Selective inductive heating of lymph. Ann Surg 1957;146:596–606.
[13] Jordan A, Scholz R, Maier-Hauff K, Johannsen M, Wust P, Nadobny J, et al. Presentation of a new magnetic field therapy system for the treatment of human solid tumors with magnetic fluid hyperthermia. J Magn Magn Mater 2001;225 (1–2):118–26.
[14] Chan DCF, Kirpotin DB, Bunn PA. Synthesis and evaluation of colloidal magnetic iron-oxides for the site-specific radiofrequency-induced hyperthermia of cancer. J Magn Magn Mater 1993;122:374–8.
[15] Jordan A, Wust P, Fahling H, John W, Hinz A, Felix R. Inductive heating of ferrimagnetic particles and magnetic fluids: Physical evaluation of their potential for hyperthermia. Int J Hyperthermia 1993;9(1):51–68.
[16] Jordan A, Scholz R, Wust P, Schirra H, Schiestel Thomas, Schmidt H, et al. Endocytosis of dextran and silan-coated magnetite nanoparticles and the effect of intracellular hyperthermia on human mammary carcinoma cells in vitro. J Magn Magn Mater 1999;194(1):185–96.
[17] Moroz P, Jones SK, Gray BN. Magnetically mediated hyperthermia: current status and future directions. Int J Hyperthermia 2002;18(4):267–84.
[18] Maier-Hauff K, Ulrich F, Nestler D, Niehoff H, Wust, Thiesen B, et al. Efficacy and safety of intratumoral thermotherapy using magnetic iron-oxide nanoparticles combined with external beam radiotherapy on patients with recurrent glioblastoma multiforme. J Neuro-Oncol 2010:1–8.
[19] Hergt R, Andra W, D'Ambly CG, Hilger I, Kaiser WA, Richter U, et al. Physical limits of hyperthermia using magnetite fine particles. IEEE Trans Magn 1998;34(5 PART 2): 37453754.
[20] Barry JW, Bookstein JJ, Alksne JF. Ferromagnetic embolization. Radiology 1981;138:341–9.
[21] Rand RW, Snow HD, Brown WJ. Thermomagnetic surgery for cancer. J Surg Res 1982;33:177–83.
[22] Rand RW, Snow HD, Elliott DG, Snyder M. Thermomagnetic surgery for cancer. Appl Biochem Biotechnol 1981;6:265–72.
[23] Maier-Hauff K, Ulrich F, Nestler D, Niehoff H, Wust P, Thiesen B, et al. Efficacy and safety of intratumoral thermotherapy using magnetic iron-oxide nanoparticles combined with external beam radiotherapy on patients with recurrent glioblastoma multiforme. J Neuro Oncol 2010:1–8.
[24] Dudeck O, Bogusiewicz K, Pinkernelle J, Gaffke G, Pech M, Wieners G, et al. Local arterial infusion of superparamagnetic iron oxide particles in hepatocellular carcinoma: a feasibility and 3.0 T MRI study. Invest Radiol 2006;41(6): 527–35.
[25] Johannsen M, Gneveckow U, Eckelt L, Feussner A, Waldfner N, Scholz R, et al. Clinical hyperthermia of prostate cancer using magnetic nanoparticles: presentation of a new interstitial technique. Int J Hyperthermia 2005;21(7):637–47.
[26] Johannsen M, Gneveckow U, Taymoorian K, Cho CH, Thiesen B, Scholz R, et al. Thermal therapy of prostate cancer using magnetic nanoparticles. Termoterapia ccer de prstata mediate el uso de nanopartculas magnticas 2007;31(6): 660–7.
[27] Johannsen M, Gneveckow U, Taymoorian K, Thiesen B, Waldofner N, Scholz R, et al. Morbidity and quality of life during thermotherapy using magnetic nanoparticles in locally recurrent prostate cancer: results of a prospective phase I trial. Int J Hyperthermia 2007;23(3):315–23.
[28] Johannsen M, Gneveckow U, Thiesen B, Taymoorian K, Cho CH, Waldufner N, et al. Thermotherapy of prostate cancer using magnetic nanoparticles: feasibility, imaging, and three-dimensional temperature distribution. Eur Urol 2007;52(6): 1653–62.
[29] Johannsen M, Thiesen B, Gneveckow U, Taymoorian K, Waldufner N, Scholz R, et al. Thermotherapy using magnetic nanoparticles combined with external radiation in an orthotopic rat model of prostate cancer. Prostate 2006;66(1): 97–104.
[30] Johannsen M, Thiesen B, Jordan A, Taymoorian K, Gneveckow U, Waldufner N, et al. Magnetic fluid hyperthermia (MFH) reduces prostate cancer growth in the orthotopic Dunning R3327 rat model. Prostate 2005;64(3):283–92.
[31] Jordan A. MagForce® Nanotherapy: with tumor-specific nanoparticles against cancer. VDI Berichte; 2005. p. 111–6.
[32] Jordan A, Maier-Hauff K. Magnetic nanoparticles for intracranial thermotherapy. J Nanosci Nanotechnol 2007;7(12):4604–6.
[33] Jordan A, Maier-Hauff K, Wust P, Rau B, Johannsen M. Thermotherapy using magnetic nanoparticles. Thermotherapie mit magnetischen nanopartikeln 2007;13(10):894–902.
[34] Jordan A, Scholz R, Maier-Hauff K, van Landeghem FKH, Waldoefner N, Teichgraeber U, et al. The effect of thermotherapy using magnetic nanoparticles on rat malignant glioma. J Neuro Oncol 2006;78(1):7–14.
[35] Maier-Hauff K, Rothe R, Scholz R, Gneveckow U, Wust P, Thiesen B, et al. Intracranial thermotherapy using magnetic nanoparticles combined with external beam radiotherapy: results of a feasibility study on patients with glioblastoma multiforme. J Neuro Oncol 2007;81(1):53–60.
[36] Morgul MH, Raschzok N, Schwartlander R, Vondran FW, Michel R, Stelter L, et al. Tracking of primary human hepatocytes with clinical MRI: initial results with Tat-peptide modified superparamagnetic iron oxide particles. Int J Artif Organs 2008;31(3):252–7.
[37] Thiesen B, Jordan A. Clinical applications of magnetic nanoparticles for hyperthermia. Int J Hyperthermia 2008;24(6):467–74.
[38] Wust P, Gneveckow U, Johannsen M, Buhmer D, Henkel T, Kahmann F, et al. Magnetic nanoparticles for interstitial thermotherapy — feasibility, tolerance and achieved temperatures. Int J Hyperthermia 2006;22(8):673–85.
[39] Johannsen M, Thiesen B, Wust P, Jordan A. Magnetic nanoparticle hyperthermia for prostate cancer. Int J Hyperthermia 2010;26(8):790–5.
[40] Morrish AH. The physical principles of magnetism. New York: IEEE Press; 2001.
[41] Frenkel J, Dorfman J. Spontaneous and induced magnetisation in ferromagnetic bodies [1]. Nature 1930;126(3173):274–5.
[42] Kittel C. Theory of the structure of ferromagnetic domains in films and small particles. Phys Rev 1946;70(11–12):965–71.
[43] Stoner EC, Wohlfarth EP. Philos Trans R Soc Lond A 1948;240:599.
[44] Neel L. Théorie du trainage magnétique des ferromagnétiques en grains fins avec applications aux terres cuites. Ann Géophys 1949;5:99–136.
[45] Brown WF. Thermal fluctuations of a single-domain particle. Phys Rev 1963;130 (5):1677–86.
[46] Gottschalk VH. Physics 1935;6:127.
[47] Elmor WC. The magnetization of ferromagnetic colloids. Phys Rev 1938;45: 1092.
[48] Bitter F, Kaufmann AR, Starr C, Pan ST. Magnetic studies of solid solutions II. The properties of quenched copper–iron alloys. Phys Rev 1941;60(2):134–8.
[49] Meyer A, Vogt E. Z Naturforsch 1952;7a:334.
[50] Heukelom W, Broeder JJ, Van Reijen LL. J Chim Phys 1954;51:474.
[51] Bean CP. Hysteresis loops of mixtures of ferromagnetic micropowders. J Appl Phys 1955;26(11):1381–3.
[52] Bean CP, Rodbell DS. Kinetics of magnetization in some square loop magnetic tapes [2]. J Appl Phys 1955;26(1):124–5.
[53] Kneller EF, Luborsky FE. Particle size dependence of coercivity and remanence of single-domain particles. J Appl Phys 1963;34(3):656–8.
[54] Leslie-Pelecky DL, Rieke RD. Magnetic properties of nanostructured materials. Chem Mater 1996;8(8):1770–83.

[55] Butler RF, Banerjee SK. Theoretical single-domain grain size range in magnetite and titanomagnetite. J Geophys Res 1975;80:4049–58.
[56] Dutz S. Nanopartikel in der Medizin. Hamburg: Verlag Dr. Kovač; 2008.
[57] Gomez RD, Luu TV, Pak AO, Kirk KJ, Chapman JN. Domain configurations of nanostructured permalloy elements. J Appl Phys 1999;85(8 II B):6163–5.
[58] Koo H, Luu TV, Gomez RD, Metlushko VV. Slow magnetization dynamics of small permalloy islands. J Appl Phys 2000;87(9 II):5114–6.
[59] Wernsdorfer W, Mailly D, Benoit A. Single nanoparticle measurement techniques. J Appl Phys 2000;87(9 II):5094–6.
[60] Wernsdorfer W, Hasselbach K, Mailly D, Barbara B, Benoit A, Thomas L, et al. DC-SQUID magnetization measurements of single magnetic particles. J Magn Magn Mater 1995;145(1–2):33–9.
[61] Martin JI, Nogues J, Liu K, Vicent JL, Schuller IK. Ordered magnetic nanostructures: fabrication and properties. J Magn Magn Mater 2003;256(1–3): 449–501.
[62] Jacobs IS, Bean CP. In: Rado GT, Suhl H, editors. Magnetism, vol. 3. New York: Academic Press; 1963. p. 271.
[63] Batlle X, Labarta A. Finite-size effects in fine particles: magnetic and transport properties. J Phys D Appl Phys 2002;35(6):R15–42.
[64] Skomski R. Nanomagnetics. J Phys Condens Matter 2003;15(20):R841–96.
[65] Chikazumi S. Physics of ferromagnetism, magnetic characteristics and engineering applications, vol. 2. Tokyo: Shokabo Publ. Co; 1984.
[66] Coffey WT, Crothers DSF, Dormann JL, Geoghegan LJ, Kalmykov YP, Waldron JT, et al. The effect of an oblique magnetic field on the superparamagnetic relaxation time. J Magn Magn Mater 1995;145(3):L263–7.
[67] Coffey WT, Crothers DSF, Kalmykov YP, Waldron JT. Constant-magnetic-field effect in Néel relaxation of single-domain ferromagnetic particles. Phys Rev B 1995;51(22):15947–56.
[68] Coffey WT, Crothers DSF, Dormann JL, Geoghegan LJ, Kalmykov YP, Waldron JT, et al. Effect of an oblique magnetic field on the superparamagnetic relaxation time. Phys Rev B 1995;52(22):15951–65.
[69] Wohlfarth EP. J Phys 1980;10:241.
[70] Wenger LE, Mydosh JA. Nonuniqueness of H23 and H2 field-temperature transition lines in spin-glasses. Phys Rev B 1984;29(7):4156–8.
[71] Yurkov GY, Gubin SP, Pankratov DA, Koksharov YA, Kozinkin AV, Spichkin YI, et al. Iron(III) oxide nanoparticles in a polyethylene matrix. Inorg Mater 2002;38(2): 137–45.
[72] Gubin SP, Spichkin YI, Koksharov YA, Yurkov GY, Kozinkin AV, Nedoseikina TI, et al. Magnetic and structural properties of Co nanoparticles in a polymeric matrix. J Magn Magn Mater 2003;265(2):234–42.
[73] Paulides MM, Bakker JF, Chavannes N, Van Rhoon GC. A patch antenna design for application in a phased-array head and neck hyperthermia applicator. IEEE Trans Biomed Eng 2007;54(11):2057–63.
[74] Paulides MM, Bakker JF, Zwamborn APM, van Rhoon GC. A head and neck hyperthermia applicator: theoretical antenna array design. Int J Hyperthermia 2007;23(1):59–67.
[75] Paulides MM, Wielheesen DHM, Van der Zee J, Van Rhoon GC. Assessment of the local SAR distortion by major anatomical structures in a cylindrical neck phantom. Int J Hyperthermia 2005;21(2):125–40.
[76] Sneed PK, Stauffer PR, McDermott MW, Diederich CJ, Lamborn KR, Prados MD, et al. Survival benefit of hyperthermia in a prospective randomized trial of brachytherapy boost ± hyperthermia for glioblastoma multiforme. Int J Radiat Oncol Biol Phys 1998;40(2):287–95.
[77] Rau B, Wust P, Tilly W, Gellermann J, Harder C, Riess H, et al. Preoperative radiochemotherapy in locally advanced or recurrent rectal cancer: regional radiofrequency hyperthermia correlates with clinical parameters. Int J Radiat Oncol Biol Phys 2000;48(2):381–91.
[78] Mahmoudi M, Sant S, Wang B, Laurent S, Sen T. Superparamagnetic iron oxide nanoparticles (SPIONs): development, surface modification and applications in chemotherapy. Adv Drug Deliv Rev 2011;63(1–2):24–46.
[79] www.magforce.de.
[80] Gordon RT, Hines JR, Gordon D. Intracellular hyperthermia. A biophysical approach to cancer treatment via intracellular temperature and biophysical alterations. Med Hypothesis 1979;5:83–102.
[81] Rosensweig RE. Heating magnetic fluid with alternating magnetic field. J Magn Magn Mater 2002;252(1–3 SPEC ISS):370–4.
[82] Le Renard PE, Buchegger F, Petri-Fink A, Bosman F, Rüfenacht D, Hofmann H, et al. Int J Hyperthermia 2009;25(3):229–39.
[83] Funovics MA, Kapeller B, Hoeller C, Su HS, Kunstfeld R, Puig S, et al. MR imaging of the her2/neu and 9.2.27 tumor antigens using immunospecific contrast agents. Magn Reson Imaging 2004;22(6):843–50.
[84] Peng XH, Qian X, Mao H, Wang AY, Chen ZG, Nie S, et al. Targeted magnetic iron oxide nanoparticles for tumor imaging and therapy. Int J Nanomedicine 2008;3 (3):311–21.
[85] Serda RE, Adolphi NL, Bisoffi M, Sillerud LO. Targeting and cellular trafficking of magnetic nanoparticles for prostate cancer imaging. Mol Imaging 2007;6(4): 277–88.
[86] Le Renard P-E, Jordan O, Faes A, Petri-Fink A, Hofmann H, Rüfenacht D, Bosman F, Buchegger F, Doelker E. The in vivo performance of magnetic particle-loaded injectable, in situ gelling, carriers for the delivery of local hyperthermia. Biomaterials 2010;31(4):691–705.
[87] Ito A, Shinkai M, Honda H, Kobayashi T. Medical application of functionalized magnetic nanoparticles. J Biosci Bioeng 2005;100(1):1–11.
[88] Häfeli UO. Magnetic nano- and microparticles for targeted drug delivery. In: Arshady R, Kono K, editors. Smart nanoparticles in nanomedicine — the MML series, vol 8. London, UK: Kentus Books; 2006. p. 77–126.
[89] Johnson RH, Robinson MP, Preece AW, Green JL, Pothecary NM, Railton CJ. Effect of frequency and conductivity on field penetration of electromagnetic hyperthermia applicators. Phys Med Biol 1993;38(8):1023–34.
[90] Van den Berg CAT, Bartels LW, De Leeuw AAC, Lagendijk JJW, Van de Kamer JB. Experimental validation of hyperthermia SAR treatment planning using MR B1+ imaging. Phys Med Biol 2004;49(22):5029–42.
[91] Brezovich IA. Low frequency hyperthermia: capacitive and ferromagnetic thermoseed methods. Med Phys Monogr Med Phys 1988;16:82.
[92] Hergt R, Dutz S, Roeder M. Effects of size distribution on hysteresis losses of magnetic nanoparticles for hyperthermia. J Phys Condens Matter 2008;20 (38).
[93] Hergt R, Dutz S, Zeisberger M. Validity limits of the Neel relaxation model of magnetic nanoparticles for hyperthermia. Nanotechnology 2010;21(1): 015706.
[94] Fortin JP, Gazeau F, Wilhelm C. Intracellular heating of living cells through Neel relaxation of magnetic nanoparticles. Eur Biophys J 2008;37(2):223–8.
[95] Müller R, Hergt R, Zeisberger M, Gawalek W. Preparation of magnetic nanoparticles with large specific loss power for heating applications. J Magn Magn Mater 2005;289:13–6.
[96] Atsumi T, Jeyadevan B, Sato Y, Tohji K. Heating efficiency of magnetite particles exposed to AC magnetic field. J Magn Magn Mater 2007;310(Suppl 2 Part 3): 2841–3.
[97] Zhang LY, Gu HC, Wang XM. Magnetite ferrofluid with high specific absorption rate for application in hyperthermia. J Magn Magn Mater 2007;311(1 SPEC ISS): 228–33.
[98] Fortin JP, Wilhelm C, Servais J, M ©nager C, Bacri JC, Gazeau F. Size-sorted anionic iron oxide nanomagnets as colloidal mediators for magnetic hyperthermia. J Am Chem Soc 2007;129(9):2628–35.
[99] Hergt R, Hiergeist R, Zeisberger M, Schüler D, Heyen U, Hilger I, et al. Magnetic properties of bacterial magnetosomes as potential diagnostic and therapeutic tools. J Magn Magn Mater 2005;293:80–6.
[100] Suto M, Hirota Y, Mamiya H, Fujita A, Kasuya R, Tohji K, et al. Heat dissipation mechanism of magnetite nanoparticles in magnetic fluid hyperthermia. J Magn Magn Mater 2009;321(10):1493–6.
[101] Pollert E, Veverka P, Veverka M, Kaman O, Z v ›ta K, Vasseur S, et al. Search of new core materials for magnetic fluid hyperthermia: preliminary chemical and physical issues. Prog Solid State Chem 2009;37(1):1–14.
[102] Mahmoudi M, Simchi A, Imani M, Milani AS, Stroeve P. Optimal design and characterization of superparamagnetic iron oxide nanoparticles coated with polyvinyl alcohol for targeted delivery and imaging. J Phys Chem B 2008;112(46): 14470–81.
[103] Hergt R, Dutz S, Muller R, Zeisberger M. Magnetic particle hyperthermia: nanoparticle magnetism and materials development for cancer therapy. J Phys Condens Matter 2006;18(38):S2919–34.
[104] Dutz S, Clement JH, Eberbeck D, Gelbrich T, Hergt R, Mueller R, et al. Ferrofluids of magnetic multicore nanoparticles for biomedical applications. J Magn Magn Mater 2009;321(10):1501–4.
[105] Richter H, Kettering M, Wiekhorst F, Steinhoff U, Hilger I, Trahms L. Magnetorelaxometry for localization and quantification of magnetic nanoparticles for thermal ablation studies. Phys Med Biol 2010;55(3):623.
[106] Janmaleki M, Mahmoudi M, Rafienia M, Peirovi H. Application potentials of microwave in nanomagnetic particle hyperthermia. IFMBE Proceedings; 2009. p. 117–9.
[107] Hergt R, Hiergeist R, Hilger I. Magnetic nanoparticles for thermoablation. Recent Res Dev Mater Sci 2002;3:723.
[108] Hergt R, Dutz S. Magnetic particle hyperthermia — biophysical limitations of a visionary tumour therapy. J Magn Magn Mater 2007;311(1):187–92.
[109] Ying-ying G, Tan Xiao-ping T, Shu-quan L, Shang-bin S. Effects of La3? doping on MnZn ferrite nanoscale particles synthesized by hydrothermal method. J Cent S Univ Tech 2004;11(2):113–228.
[110] Sawatzky GA, Van Der Woude F, Morrish AH. Cation distributions in octahedral and tetrahedral sites of the ferrimagnetic spinel $CoFe_2O_4$. J Appl Phys 1968;39 (2):1204–5.
[111] Kuznetsov OA, Sorokina ON, Leontiev VG, Shlyakhtin OA, Kovarski AL, Kuznetsov AA. ESR study of thermal demagnetization processes in ferromagnetic nanoparticles with Curie temperatures between 40 and 60 °C. J Magn Magn Mater 2007;311(1 SPEC ISS):204–7.
[112] Pollert E. Crystal chemistry of magnetic oxides part 2: hexagonal ferrites. Prog Crystal Growth Characterization 1985;11(3):155–205.
[113] Auzans E, Zins D, Blums E, Massart R. Synthesis and properties of Mn–Zn ferrite ferrofluids. J Mater Sci 1999;34:1253–60.
[114] Sharma R, Chen CJ. Newer nanoparticles in hyperthermia treatment and thermometry. J Nanopart Res 2009;11:671–89.
[115] Brusentsova TN, Kuznetsov VD. Synthesis and investigation of magnetic properties of substituted ferrite nanoparticles of spinel system $Mn_{1-x}Zn_x[Fe_{2-y}L_y]O_4$. J Magn Magn Mater 2007;311(1):22–5.
[116] Sutariya GM, Vincent D, Bayard B, Upadhyay RV, Noyel G, Mehta RV. Magnetic DC field and temperature dependence on complex microwave magnetic permeability of ferrofluids: effect of constituent elements of substituted Mn ferrite. J Magn Magn Mater 2003;260(1–2):42–7.
[117] Shuai J, Parker I. Optical single-channel recording by imaging Ca^{2+} flux through individual ion channels: theoretical considerations and limits to resolution. Cell Calcium 2005;37(4):283–99.
[118] Bretcanu O, Verné E, Cöisson M, Tiberto P, Allia P. Magnetic properties of the ferrimagnetic glass-ceramics for hyperthermia. J Magn Magn Mater 2006;305 (2):529–33.

[119] Weller D, Moser A, Folks L, Best ME, Lee W, Toney MF, et al. High K_u materials approach to 100 gbits/in^2. IEEE Trans Magn 2000;36(1 PART 1):10–5.
[120] Brusentsov NA, Brusentsova TN, Sergeev AV, Shumakov LI. Ferrimagnetic fluids and ferro- and ferrimagnetic suspensions for the RF-induction hyperthermia of tumors. Pharm Chem J 2000;34(4):201–7.
[121] Brusentsov NA, Komissarova LK, Brusentsova TN, Baiburtskii FS, Mironov AF, Lyubeshkin AV, et al. Molecular-biological problems of drug design and mechanism of drug action: cytotoxicity of photoheme-containing ferrimagnetic fluid in alternating magnetic field. Pharm Chem J 2005;39(3):113–8.
[122] Brusentsova TN, Brusentsov NA, Kuznetsov VD, Nikiforov VN. Synthesis and investigation of magnetic properties of Gd-substituted Mn–Zn ferrite nanoparticles as a potential low-TC agent for magnetic fluid hyperthermia. J Magn Magn Mater 2005;293(1):298–302.
[123] Settecase F, Sussman MS, Roberts TPL. A new temperature-sensitive contrast mechanism for MRI: Curie temperature transition-based imaging. Contrast Media Mol Imaging 2007;2:50–4.
[124] Duong GV, Turtelli RS, Nunes WC, Schafler E, Hanh N, Grössinger R, et al. Ultrafine $Co_{1-x}Zn_xFe_2O_4$ particles synthesized by hydrolysis: effect of thermal treatment and its relationship with magnetic properties. J NonCrystalline Solids 2007;353(8–10):805–7.
[125] Tannenwald PE. Multiple resonances in cobalt ferrite. Phys Rev 1995;99(2):463–4.
[126] Shirk BT, Buessem WR. Temperature dependence of M_s and K_1 of $BaFe_{12}O_{19}$ and $SrFe_{12}O_{19}$ single crystals. J Appl Phys 1969;40(3):1294–6.
[127] Mahmoudi M, Milani AS, Stroeve P. Surface architecture of superparamagnetic iron oxide nanoparticles for application in drug delivery and their biological response: a review. Int J Biomed Nanosci Nanotechnol 2010;1(2/3/4):164–201.
[128] Mahmoudi M, Simchi A, Imani M. Recent advances in surface engineering of superparamagnetic iron oxide nanoparticles for biomedical applications. J Iran Chem Soc 2010;7:S1–S27.
[129] Shubayev VI, Pisanic TR, Jin S. Magnetic nanoparticles for theragnostics. Adv Drug Deliv Rev 2009;61:467–77.
[130] Mahmoudi M, Hosseinkhani H, Hosseinkhani M, Boutry S, Simchi A, Journeay WS, et al. Magnetic resonance imaging tracking of stem cells in vivo using iron oxide nanoparticles as a tool for the advancement of clinical regenerative medicine. Chem Rev 2011;111(2):253–80.
[131] Mahmoudi M, Shokrgozar MA, Simchi A, Imani M, Milani AS, Stroeve P, et al. Multiphysics flow modeling and in vitro toxicity of iron oxide nanoparticles coated with poly(vinyl alcohol). J Phys Chem C 2009;113(6):2322–31.
[132] Mahmoudi M, Simchi A, Imani M. Cytotoxicity of uncoated and polyvinyl alcohol coated superparamagnetic iron oxide nanoparticles. J Phys Chem C 2009;113(22):9573–80.
[133] Mahmoudi M, Simchi A, Imani M, Häfeli UO. Superparamagnetic iron oxide nanoparticles with rigid cross-linked polyethylene glycol fumarate coating for application in imaging and drug delivery. J Phys Chem C 2009;113(19):8124–31.
[134] Mahmoudi M, Simchi A, Imani M, Milani AS, Stroeve P. An in vitro study of bare and poly(ethylene glycol)-co-fumarate-coated superparamagnetic iron oxide nanoparticles: a new toxicity identification procedure. Nanotechnology 2009;20(22):225104.
[135] Mahmoudi M, Simchi A, Imani M, Shokrgozar MA, Milani AS, Hafeli UO, et al. A new approach for the in vitro identification of the cytotoxicity of superparamagnetic iron oxide nanoparticles. Colloids Surf B Biointerfaces 2010;75(1):300–9.
[136] Mahmoudi M, Simchi A, Milani AS, Stroeve P. Cell toxicity of superparamagnetic iron oxide nanoparticles. J Colloid Interface Sci 2009;336(2):510–8.
[137] Mahmoudi M, Simchi A, Vali H, Imani M, Shokrgozar MA, Azadmanesh K, et al. Cytotoxicity and cell cycle effects of bare and poly(vinyl alcohol)-coated iron oxide nanoparticles in mouse fibroblasts. Adv Eng Mater 2009;11(12):B243–50.
[138] Mahmoudi M, Azadmanesh K, et al. Effect of nanoparticles on the cell life cycle. Chemical Reviews 2011;111(5):3407–32.
[139] Mahmoudi M, Sardari S, Shokrgozar MA, Laurent S, Stroeve P., Interaction of superparamagnetic iron oxide nanoparticles with human transferrin: Irreversible changes in human transferrin conformation. Nanoscale 2010 Revised.
[140] Mahmoudi M, Simchi A, Imani M, Stroeve P, Sohrabi A. Templated growth of superparamagnetic iron oxide nanoparticles by temperature programming in the presence of poly(vinyl alcohol). Thin Solid Films 2010;518(15):4281–9.
[141] Karlsson HL, Cronholm P, Gustafsson J, Muller L. Copper oxide nanoparticles are highly toxic: a comparison between metal oxide nanoparticles and carbon nanotubes. Chem Res Toxicol 2008;21(9):1726–32.
[142] Gupta AK, Gupta M. Synthesis and surface engineering superparamagnetic iron oxide nanoparticles for drug delivery and cellular targeting. Handbook of Particulate Drug Delivery. USA: American Scientific Publishers; 2007.
[143] Bertin A, Steibel J, Michou-Gallani AI, Gallani JL, Felder-Flesch D. Development of a dendritic manganese-enhanced magnetic resonance imaging (MEMRI) contrast agent: synthesis, toxicity (in vitro) and relaxivity (in vitro, in vivo) studies. Bioconjug Chem 2009;20(4):760–7.
[144] Maurer-Jones MA, Bantz KC, Love SA, Marquis BJ, Haynes CL. Toxicity of therapeutic nanoparticles. Nanomedicine 2009;4(2):219–41.
[145] Moore A, Weissleder R, Bogdanov Jr A. Uptake of dextran-coated monocrystalline iron oxides in tumor cells and macrophages. J Magn Reson Imaging 1997;7(6):1140–5.
[146] Corr SA, Rakovich YP, Gun'ko YK. Multifunctional magnetic-fluorescent nanocomposites for biomedical applications. Nanoscale Res Lett 2008;3:87–104.
[147] Zhao YM, Su B, Yang XJ, Tang L, Zhou CC. Study on angiogenesis-targeting peptide modified iron oxide nanoparticles used in local magnetic hyperthermia in tumor-bearing nude mouse models. Tumor 2010;30(5):370–5.
[148] Meenach SA, Hilt JZ, Anderson KW. Poly(ethylene glycol)-based magnetic hydrogel nanocomposites for hyperthermia cancer therapy. Acta Biomater 2010;6(3):1039–46.
[149] Zhang G, Liao Y, Baker I. Surface engineering of core/shell iron/iron oxide nanoparticles from microemulsions for hyperthermia. Mater Sci Eng C 2010;30(1):92–7.
[150] Balivada S, Rachakatla RS, Wang H, Samarakoon TN, Dani RK, Pyle M, et al. A/C magnetic hyperthermia of melanoma mediated by iron(0)/iron oxide core/shell magnetic nanoparticles: a mouse study. BMC Cancer 2010;10.
[151] Benkoski JJ, Patrone JJ, Crookston J, Le H, Sample J. The effects of chemical functionalization vs. biological functionalization on nanoparticle binding affinity. Materials Research Society Symposium Proceedings; 2008. p. 20–3.
[152] Goya GF, Graz V, Ibarra MR. Magnetic nanoparticles for cancer therapy. Curr Nanosci 2008;4(1):1–16.
[153] Brazel CS. Magnetothermally-responsive nanomaterials: combining magnetic nanostructures and thermally-sensitive polymers for triggered drug release. Pharm Res 2009;26(3):644–56.
[154] Peppas NA, Huang Y, Torres-Lugo M, Ward JH, Zhang J. Physicochemical foundations and structural design of hydrogels in medicine and biology. Annu Rev Biomed Eng 2000;2:9–29.
[155] Brannon-Peppas L, Blanchette JO. Nanoparticle and targeted systems for cancer therapy. Adv Drug Deliv Rev 2004;56(11):1649–59.
[156] El-Aneed A. An overview of current delivery systems in cancer gene therapy. J Control Release 2004;94(1):1–14.
[157] Ang KL, Venkatraman S, Ramanujan RV. Magnetic PNIPA hydrogels for hyperthermia applications in cancer therapy. Mater Sci Eng C 2007;27(3):347–51.
[158] Carroll KS, McKinney JB, Johnson DT, Brazel CS. Development of magnetothermal responsive systems for tumor treatment. Proc Int Symp Control Rel Bioact Mater 2003;30:82–3.
[159] Shinkai M, Yanase M, Honda H, Wakabayashi T, Yoshida J, Kobayashi T. Intracellular hyperthermia for cancer using magnetite cationic liposome: in vitro study. Jpn J Cancer Res 1996;87:1179–83.
[160] Suzuki M, Shinkai M, Honda H, Kobayashi T. Anticancer effect and immune induction by hyperthermia of malignant melanoma using magnetite cationic liposomes. Melanoma Res 2003;13:129–35.
[161] Yanase M, Shinkai M, Honda H, Wakabayashi T, Yoshida J, Kobayashi T. Intracellular hyperthermia for cancer using magnetite cationic liposomes: an in vivo study. Jpn J Cancer Res 1998;89:463–9.
[162] Matsuoka F, Shinkai M, Honda H, Kubo T, Sugita T, Kobayashi T. Hyperthermia using magnetite cationic liposomes for hamster osteosarcoma. Biomagn Res Technol 2004;2:3–4.
[163] Matsuno H, Tohnai I, Mitsudo K, Hayashi Y, Ito M, Shinkai M, et al. Interstitial hyperthermia using magnetite cationic liposomes inhibit to tumor growth of VX-7 transplanted tumor in rabbit tongue. Jpn J Hyperthermic Oncol 2001;17:141–9.
[164] Le B, Shinkai M, Kitade T, Honda H, Yoshida J, Wakabayashi T, et al. Preparation of tumorspecific magnetoliposomes and their application for hyperthermia. J Chem Eng Jpn 2001;34:66–72.
[165] Shinkai M, Le B, Honda H, Yoshikawa K, Shimizu K, Saga S, et al. Targeting hyperthermia for renal cell carcinoma using human MN antigen-specific magnetoliposomes. Jpn J Cancer Res 2001;92:1138–45.
[166] Lu Z, Prouty MD, Quo Z, Golub VO, Kumar CSSR, Lvov YM. Magnetic switch of permeability for polyelectrolyte microcapsules embedded with Co@Au nanoparticles. Langmuir 2005;21(5):2042–50.
[167] Masai A. Development of anticancer-agent-releasing microcapsules for chemotherapy combined with embolo-hyperthermic therapy. Nippon Igaku Hoshasen Gakkai Zasshi 1995;55(1):50–7.
[168] Sato T, Masai A, Ota Y, Sato H, Matuski H, Yanada T, et al. Development of anticancer agent releasing microcapsule made of ferromagnetic amorphous flakes for intratissue hyperthermia. IEEE Trans Magn 1993;29(6 pt 2):3325–30.
[169] Jang J-T, Nah H, Lee J-H, Moon SH, Kim MG, Cheon J. Critical enhancements of MRI contrast and hyperthermic effects by dopant-controlled magnetic nanoparticles. Angew Chem Int Ed 2009;48(7):1234–8.
[170] Lee J-H, Huh Y-M, Jun Y-W, Seo J-W, Jang J-T, Song H-T, et al. Artificially engineered magnetic nanoparticles for ultra-sensitive molecular imaging. Nat Med 2007;13(1):95–9.
[171] Liu C, Zou B, Rondinone AJ, Zhang ZJ. Chemical control of superparamagnetic properties of magnesium and cobalt spinel ferrite nanoparticles through atomic level magnetic couplings. J Am Chem Soc 2000;122(26):6263–7.
[172] Ge J, Hu Y, Biasini M, Beyermann WP, Yin Y. Superparamagnetic magnetite colloidal nanocrystal clusters. Angew Chem 2007;119:4420–3.
[173] Ge J, Hu Y, Yin Y. Highly tunable superparamagnetic colloidal photonic crystals. Angew Chem Int Ed 2007;46:7428–31.
[174] Amiri H, Mahmoudi M, Lascialfari A. Superparamagnetic colloidal nano-crystals coated with polyethylene glycol fumarate coated: a possible novel theranostic agent. Nanoscale 2011;3(3):1022–30.
[175] Nakashima S, Fujita K, Tanaka K, Hirao K. High magnetization and the high-temperature superparamagnetic transition with intercluster interaction in disordered zinc ferrite thin film. J Phys Condens Matter 2005;17(1):137–49.
[176] Drake P, Cho H-J, Shih P-S, Kao C-H, Lee K-F, Kuo C-H, et al. Gd-doped iron-oxide nanoparticles for tumour therapy via magnetic field hyperthermia. J Mater Chem 2007;17:4914–8.
[177] Bárcena C, Sra AK, Chaubey GS, Khemtong C, Liu JP, Gao J. Zinc ferrite nanoparticles as MRI contrast agents. Chem Commun (Camb) 2008;19:2224–6.
[178] Maswadi SM, Dodd SJ, Gao JH, Glickman RD. Temperature mapping of laser-induced hyperthermia in an ocular phantom using magnetic resonance thermography. J Biomed Opt 2004;9(4):711–8.

[179] Amao Y, Okura I. Fullerene C60 immobilized in polymethylmethacrylate film as an optical temperature sensing material. Analysis 2000;28:847–9.
[180] Maqueda RJ, Wurden GA, Terry JL, Stillerman JA. The new infrared imaging system on Alcator C-Mod. Rev Sci Instrum 2000;70:734–7.
[181] Romanus E, Berkov DV, Prass S, Grob C, Weitschies W, Weber P. Determination of energy barrier distributions of magnetic nanoparticles by temperature dependent magnetorelaxometry. Nanotechnology 2003;14:1251–4.
[182] Le Bihan DL, Delannoy J, Levin RL. Temperature mapping with MR imaging of molecular diffusion: application to hyperthermia. Radiology 1989;171:853–7.
[183] www.sennewald.de.
[184] Yamaoka T, Tabata Y, Ikada Y. J Pharm Sci 1994;83:6.
[185] Li P, Zhu AM, Liu QL, Zhang QG. Fe_3O_4/poly(N-isopropylacrylamide)/chitosan composite microspheres with multiresponsive properties. Ind Eng Chem Res 2008;47(20):7.
[186] Chen T-J, Cheng T-H, Chen C-Y, Hsu SCN, Cheng T-L, Liu G-C, et al. Targeted Herceptin–dextran iron oxide nanoparticles for noninvasive imaging of HER2/neu receptors using MRI. J Biol Inorg Chem 2009;14:253–60.
[187] Tian J, Feng YK, Xu YS. Ring opening polymerization of D,L-lactide on magnetite nanoparticles. Macromol Res 2006;14(2):5.
[188] Ruiz JM, Benoit JP. J Control Release 1991;86(8):5.
[189] Chen KL, Mylon SE, Elimelech M. Aggregation kinetics of alginate-coated hematite nanoparticles in monovalent and divalent electrolytes. Environ Sci Technol 2006;40(5):1516–23.
[190] Gurny R, Ibrahim H, Aebi A, Buri P, Wilson CG, Washington N, et al. Design and evaluation of controlled release systems for the eye. J Control Release 1987;6:367–73.
[191] Saettone MF, Chetoni P, Torracca MT, Burgalassi S, Giannaccini B. Evaluation of muco-adhesive properties and in vivo activity of ophthalmic vehicles based on hyaluronic acid. Int J Pharm 1989;51:203–12.
[192] Lehr CM, Bouwstra JA, Schacht EH, Junginger HE. In vitro evaluation of mucoadhesive properties of chitosan and some other natural polymers. Int J Pharm 1992;78:43–8.
[193] Durrani AM, Farr SJ, Kellaway IW. Influence of molecular weight and formulation pH on the precorneal clearance rate of hyaluronic acid in the rabbit eye. Int J Pharm 1995;118:243–50.
[194] Zimmer A, Chetoni P, Saettone MF, Zerbe H, Kreuter j. Evaluation of pilocarpine-loaded albumin particles as controlled drug delivery systems for the eye. II. Co-administration with bioadhesive and viscous polymers. J Control Release 1995;33:31–46.
[195] Tamer U, Gundogdu Y, Boyaci IH, Pekmez K. Synthesis of magnetic core–shell Fe_3O_4–Au nanoparticle for biomolecule immobilization and detection. J Nanopart Res 2009, doi:10.1007/s11051-009-9749-0.
[196] Lu CW, Hung Y, Hsiao JK, Yao M, Chung TH, Lin YS, et al. Bifunctional magnetic silica nanoparticles for highly efficient human stem cell labeling. Nano Lett 2007;7(1):149–54.
[197] Dodd CH, Hsu HC, Chu WJ, Yang P, Zhang HG, Mountz JD, et al. Normal T-cell response and in vivo magnetic resonance imaging of T cells loaded with HIV transactivator-peptide-derived superparamagnetic nanoparticles. J Immunol Methods 2001;256(1–2):89–105.
[198] Kumagai M, Kano MR, Morishita Y, Ota M, Imai Y, Nishiyama N, et al. Enhanced magnetic resonance imaging of experimental pancreatic tumor in vivo by block copolymer-coated magnetite nanoparticles with TGF-β inhibitor. J Control Release 2009;140(3):306–11.
[199] Wu YJ, Muldoon LL, Varallyay C, Markwardt S, Jones RE, Neuwelt EA. In vivo leukocyte labeling with intravenous ferumoxides/protamine sulfate complex and in vitro characterization for cellular magnetic resonance imaging. Am J Physiol Cell Physiol 2007;293:C1698–708.
[200] Laurent S, Bridot JL, Elst LV, Muller RN. Magnetic iron oxide nanoparticles for biomedical applications. Future Med Chem 2010;2(3):427–49.
[201] Dimitrov I, Trzebicka B, Muller AHE, Dworak A, Tsvetanov CB. Thermosensitive water-soluble copolymers with doubly responsive reversibly interacting entities. Prog Polym Sci 2007;32:1275–343.
[202] Brazel CS, Peppas NA. Pulsatile local delivery of thrombolytic and antithrombotic agents using poly(N-isopropylacrylamide-co-methacrylic acid) hydrogels. J Control Release 1996;39:57–64.
[203] Chilkoti A, Dreher MR, Meyer DE, Raucher D. Targeted drug delivery by thermally responsive polymers. Adv Drug Deliv Rev 2002;54:613–30.
[204] Ballauff M, Lu Y. "Smart" nanoparticles: preparation, characterization and applications. Polymer 2007;48:1815–23.
[205] Klouda L, Mikos AG. Thermoresponsive hydrogels in biomedical applications. Eur J Pharm Biopharm 2008;68:34–45.
[206] Jeong B, Kim SW, Bae YH. Thermosensitive sol–gel reversible hydrogels. Adv Drug Deliv Rev 2002;54:37–51.
[207] Ruel-Gariepy E, Leroux JC. In situ-forming hydrogels—review of temperature-sensitive systems. Eur J Pharm Biopharm 2004;58:409–26.
[208] Kono K. Thermosensitive polymer-modified liposomes. Adv Drug Deliv Rev 2001;53:307–19.
[209] Zhang C, Johnson DT, Brazel CS. Numerical study on the multi-region bio-heat equation to model Magnetic Fluid Hyperthermia (MFH) using low curie temperature nanoparticles. IEEE Trans Nanobiosci 2008;7(4):267–75.
[210] Meenach SA, Anderson KW, Hilt JZ. Synthesis and characterization of thermo-responsive poly(ethylene glycol)-based hydrogels and their magnetic nanocomposites. J Polym Sci A Polym Chem 2010;48(15):3229–35.
[211] Cheng S-X, Zhang J-T, Zhuo R-X. Macroporous poly(N-isopropylacrylamide) hydrogels with fast response rates and improved protein release properties. J Biomed Mater Res A 2003;67(1):96–103.
[212] Liu Q, Zhang P, Qing A, Lan Y, Lu M. Poly(N-isopropylacrylamide) hydrogels with improved shrinking kinetics by RAFT polymerization. Polymer 2006;47:2330–6.
[213] Wu C, Wang X. Globule-to-coil transition of a single homopolymer chain in solution. Phys Rev Lett 1998;80(18):4092–4.
[214] Hellweg T, Dewhurst CD, Eimer W, Kratz K. PNIPAM-co-polystyrene core–shell microgels: structure, swelling behavior, and crystallization. Langmuir 2004;20(11):4330–5.
[215] Cho CS, Cheon JB, Jeong YI, Kim IS, Kim SH, Akaike T. Novel core–shell type thermo-sensitive nanoparticles composed of poly(benzyl L-glutamate) as the core and poly(N-isopropylacrylamide) as the shell. Macromol Rapid Commun 1997;18(5):361–9.
[216] Jones CD, Lyon LA. Dependence of shell thickness on core compression in acrylic acid modified poly(N-isopropylacrylamide) core/shell microgels. Langmuir 2003;19(11):4544–7.
[217] Hasan E, Zhang M, Muller AHE, Tsvetanov CB. Thermoassociative block copolymers of poly(N-isopropylacrylamide) and poly(propylene oxide). J Macromol Sci A Pure Appl Chem 2004;A 41:467–86.
[218] Xie X, Hogen-Esch TE. Anionic synthesis of narrow molecular weight distribution water-soluble poly(N, N-dimethylacrylamide) and poly(N-acryloyl-N′-methylpiperazine). Macromolecules 1996;29:1746–52.
[219] Ishizone T, Yoshimura K, Hirao A, Nakahama S. Controlled anionic polymerization of tert-butyl acrylate with diphenylmethyl anions in the presence of dialkylzinc. Macromolecules 1998;31:8706–12.
[220] Mortensen K, Brown W. Poly(ethylene oxide)–poly(-propylene oxide)–poly (ethylene oxide) triblock copolymers in aqueous solution. The influence of relative block size. Macromolecules 1993;26:4128–35.
[221] Price CC. Polyethers. Acc Chem Res 1974;7:294–301.
[222] Aida T, Maehowa Y, Asuno S, Inoue S. "Immortal" polymerization. Polymerization of epoxide and b-lactone with aluminum porphyrin in the presence of protic compound. Macromolecules 1998;21:1195–202.
[223] Miyamoto M, Sawamoto M, Higashimura T. Living polymerization of isobutyl vinyl ether with hydrogen iodide/iodine initiating system. Macromolecules 1984;17:265–8.
[224] Sugihara S, Hashimoto K, Okabe S, Shibayama M, Kanaoka S, Aoshima S. Stimuli-responsive diblock copolymers by living cationic polymerization: precision synthesis and highly sensitive physical gelation. Macromolecules 2004;37:336–43.
[225] Ngai T, Behrens SH, Auweter H. Novel emulsions stabilized by pH and temperature sensitive microgels. Chem Commun 2005;3:331–3.
[226] Hoare T, Pelton R. Functional group distributions in carboxylic acid containing poly(N-isopropylacrylamide) microgels. Langmuir 2004;20(6):2123–33.
[227] Hoare T, Pelton R. Highly pH and temperature responsive microgels functionalized with vinylacetic acid. Macromolecules 2004;37(7):2544–50.
[228] Mertoglu M, Garniera S, Laschewsky A, Skrabania K, Storsberg J. Stimuli responsive amphiphilic block copolymers for aqueous media synthesised via reversible addition fragmentation chain transfer polymerisation (RAFT). Polymer 2005;46:7726–40.
[229] Dimitrov P, Rangelov S, Dworak A, Tsvetanov CB. Synthesis and associating properties of poly(ethoxyethyl glycidyl ether)/poly(propylene oxide) triblock copolymers. Macromolecules 2004;37:1000–8.
[230] Hayashi K, Ono K, Suzuki H, Sawada M, Moriya M, Sakamoto W, et al. ACS Appl Mater Interfaces 2010;2(7):1903–11.
[231] Si HY, Li DP, Wang TM, Zhang HL, Ren FY, Xu ZG, et al. J Nanosci Nanotechnol 2010;10(4):2325–31.
[232] Muqbil I, Masood A, Sarkar FH, Mohammad RM, Azmi AS. Progress in nanotechnology based approaches to enhance the potential of chemopreventive agents. Cancers 2011;3:428–45.
[233] Du Y, Zhang D, Liu H, Lai R. BMC Biotechnol 2009;9:84.
[234] Tseng HY, Lee GB, Lee CY, Shih YH, Lin XZ. IET Nanobiotechnol 2009;3(2):46–54.
[235] Bruners P, Braunschweig T, Hodenius M, Pietsch H, Penzkofer T, Baumann M, et al. Cardiovasc Intervent Radiol 2010;33(1):127–34.
[236] Salloum M, Ma RH, Weeks D, Zhu L. Controlling nanoparticle delivery in magnetic nanoparticle hyperthermia for cancer treatment: experimental study in agarose gel. Int J Hyperthermia 2008;24:337–45.
[237] Alexiou C, Schmid R, Jurgons R, Kremer M, Wanner G, Bergemann C, et al. Targeting cancer cells: magnetic nanoparticles as drug carriers. Eur Biophys J 2006;35(5):446–50.
[238] Nel AE, M¤dler L, Velegol D, Xia T, Hoek EMV, Somasundaran P, et al. Understanding biophysicochemical interactions at the nano-bio interface. Nat Mater 2009;8(7):543–57.
[239] Stella B, Arpicco S, Peracchia MT, Desmaële D, Hoebeke J, Renoir M, et al. Design of folic acid-conjugated nanoparticles for drug targeting. J Pharm Sci 2000;89(11):1452–64.